

# Ideal pairing of the Stokes and anti-Stokes photons in the Raman process

Kishore Thapliyal<sup>1,\*</sup> and Jan Peřina, Jr.<sup>2,†</sup>

<sup>1</sup>*Joint Laboratory of Optics of Palacký University and Institute of Physics of CAS,  
Faculty of Science, Palacký University, 17. listopadu 12, 771 46 Olomouc, Czech Republic*

<sup>2</sup>*Joint Laboratory of Optics of Palacký University and Institute of Physics of CAS,  
Institute of Physics, Czech Academy of Sciences,  
17. listopadu 50a, 771 46 Olomouc, Czech Republic*

A quantum model of the Raman process with the independent Stokes and anti-Stokes nonlinear interactions is developed to study nonclassical correlations between the photons in the Stokes and anti-Stokes fields. The role of the laser pump amplitude, the ratio of the Stokes and anti-Stokes coupling constants and the population and losses of the vibrational mode in forming the correlations is elucidated. The  $g^{(2)}$  intensity cross-correlation function, noise-reduction-factor, two-mode principal squeezing variance, logarithmic negativity, non-classicality depth, steering parameter and the Bell parameter are analyzed side-by-side to shed light to the correlations between the Stokes and anti-Stokes fields. Conditions for having the Stokes and anti-Stokes fields composed of only photon pairs, similarly as it occurs in twin beams in parametric down-conversion, are revealed. They allow for nonzero mean thermal phonon numbers.

## I. INTRODUCTION

With the recent development in various areas of quantum technology [1] search for new physical systems or processes able to generate useful quantum states has escalated. These quantum states are endowed with specific properties not available when only classical states are considered. Negative values of the Glauber-Sudarshan phase-space quasi-distribution  $P$  [2, 3] represent their most important feature from which their specific properties originate. Entangled states with genuine quantum correlations represent the most important class of such states. They cannot be written as a product of states of each subsystem. This means that the entangled states exhibit nonlocal correlations. In their simplest form of entangled photon pairs, they have been found useful, e.g., in quantum teleportation [4], dense coding [5], metrology [6] and cryptography [7]. Even stronger quantum correlations between two photons, known as the Einstein-Podolsky-Rosen (EPR) steering and the Bell non-locality, exist and they have been applied, e.g., in device-independent quantum cryptography [8, 9]. Also the quantum states with greater numbers of photons, exhibiting correlations in photon numbers have been studied recently using photon-number-resolving detection ([10] and references therein).

The process of parametric down-conversion is traditionally used to generate various kinds of quantum (entangled) states [11]. Nevertheless, other nonlinear processes, like the Raman process [12] or the four-wave mixing [13], are also endowed with the capability to generate quantum states [14]. On one side these third-order nonlinear processes are weaker than parametric down-conversion. On the other side, they are more complex as

they involve four interacting fields and so they are more flexible in the generation of quantum states. Here, we concentrate our attention to the Raman process, in which the Stokes and anti-Stokes photons are generated, similarly as the signal and idler photons emerge in parametric down-conversion. However, there is a principal difference in the microscopic nature of both processes. Whereas the signal and idler photons emerge as a photon pair in one quantum event, the Stokes and anti-Stokes photons originate in two quantum events, the first in the Stokes interaction and the second in the anti-Stokes interaction of the whole Raman process [14, 15]. The quantum correlations between the Stokes and anti-Stokes photons are mediated by the phonons of the vibrational mode that participates in both interactions. The correlations are established by phonons that are produced in the Stokes interaction together with the Stokes photons and later disappear in the anti-Stokes interaction leaving the anti-Stokes photons. Owing to this microscopic mechanism, the correlations between the Stokes and anti-Stokes modes are influenced by detailed conditions of the Raman process and, as a consequence, these correlations do not have to be strong, or even quantum. On the other hand, the more complex microscopic mechanism of the Raman process allows us to obtain states not attainable in parametric down-conversion.

Correlations between the Stokes and anti-Stokes modes in the Raman process have been theoretically studied in [14, 15]. The quantum theory of the Raman process was introduced in [16] and the generation of several types of the nonclassical states was discussed over the time (for the review, see [17, 18]). Recently, the correlations between the optical and phonon modes both at resonance and out-of resonance, as well as the generalization of the Raman process to the hyper-Raman process have been investigated [19–21]. The fields in the Raman process were experimentally investigated in inelastic scattering of the laser light from water [22], Rb vapors [23] and diamond [24]. The light scattered from diamond exhibited

\* kishore.thapliyal@upol.cz

† jan.perina.jr@upol.cz

the Bell nonlocal correlations [25].

The Raman process is also investigated under the conditions in which we have a large number of non-resonant weakly-interacting vibrational modes, instead of one strongly-interacting resonant vibrational mode. In this case the correlations in the Stokes and anti-Stokes fields emerge due to the exchange of virtual phonons [26]. Successful theory describing this process is based upon the unitary transformation that introduces photon pairs as quasi-particles, in close analogy with the transformation that reveals the Cooper pairs in superconductivity [27, 28]. As there occurs no distinct vibrational frequency in the interaction, the spectra of the emitted Stokes and anti-Stokes fields are broad without peaks. The Stokes and anti-Stokes photons are ideally paired and there occurs the entanglement in their frequencies. Such Raman process exhibits many features typical of four-wave mixing [13]. It has been extensively studied in Refs. [26–28].

We note that the Raman process in the form of inelastic scattering (the Raman scattering) of photons from molecules, has been used to build a quantum memory [29–31], perform long distance quantum communication [32], quantum state transfer between the light and matter [33], entangle remote super-conducting circuits [34], generate single photons [35], photon-phonon correlated pairs [36] and other nonclassical states [37–40]. Also, the Raman scattering is frequently observed as an unwanted source of the noise, e.g., in the wavelength-multiplexed quantum cryptographic systems [41] or in photon-pair generation in optical fibers via the four-wave mixing [42–44].

Being inspired by the above applications of the Raman process in quantum information tasks, we study quantum as well as classical correlations between the Stokes and anti-Stokes modes using the quantum model of the Raman process with one distinct vibrational mode and the strong coherent pump beam. Using the appropriate nonlinear momentum operator that involves the independent Stokes and anti-Stokes interactions we derive the corresponding Heisenberg equations. Their solution then allows us to determine the field characteristics including the intensity cross-correlation functions, the logarithmic negativity, the EPR steering parameters and the Bell parameter under typical conditions. They are compared with those characterizing ideal twin beams composed only of photon pairs and originating in parametric down-conversion under the conditions similar to those in the Raman process. In the Raman process, among others, we address the role of damping of the vibrational mode and the amount of thermal phonons present naturally in this mode.

The paper is organized as follows. We introduce the quantum model of the Raman process and solve its dynamics in Sec. II. Various parameters quantifying two-mode correlations are discussed in Sec. III. A simplified model of the Raman process is analytically treated in Sec. IV considering the initial vacuum vibrational mode. The model elucidating the role of non-zero initial mean

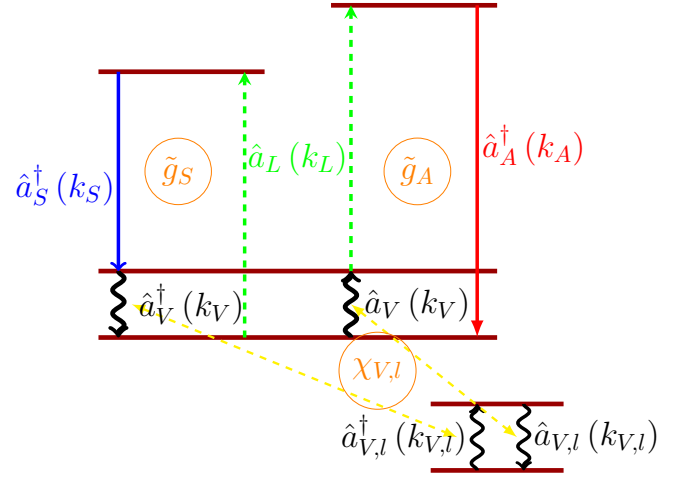


FIG. 1. Schematic diagram of the model of the Raman process: A photon in pump mode with wave vector  $k_L$  with annihilation operator  $\hat{a}_L$  is either converted into a phonon with wave vector  $k_V$  and annihilation operator  $\hat{a}_V$  and a Stokes photon with wave vector  $k_S$  and annihilation operator  $\hat{a}_S$  (Stokes interaction with coupling constant  $\tilde{g}_S$ ) or is annihilated together with a phonon to give rise to an anti-Stokes photon with wave vector  $k_A$  and annihilation operator  $\hat{a}_A$  (anti-Stokes interaction with coupling constant  $\tilde{g}_A$ ). Inversion processes also occur. The vibrational mode with phonons are further damped via their interaction with reservoir phonon modes with wave vectors  $k_{V,l}$  and annihilation operators  $\hat{a}_{V,l}$  (linear coupling constants  $\chi_{V,l}$ ).

phonon numbers is presented in Sec. V. The general discussion that takes into account the phonon losses and thermal reservoir phonons is given in Sec. VI. Conclusions are drawn in Sec. VII.

## II. QUANTUM MODEL OF THE RAMAN PROCESS

We consider the monochromatic waves in the laser (frequency  $\omega_L$ , wave vector  $k_L$ ), Stokes ( $\omega_S$ ,  $k_S$ ), anti-Stokes ( $\omega_A$ ,  $k_A$ ), and vibration ( $\omega_V$ ,  $k_V$ ) modes that propagate along a nonlinear crystal of length  $L$  and mutually interact in the Raman process described in the scheme of Fig. 1. Moreover, the laser pump beam is assumed to have a strong classical amplitude  $|\alpha_L| \exp(i\phi_L)$  which results in the following nonlinear momentum operator  $\hat{G}(z)$ :

$$\begin{aligned} \hat{G}(z) = & \hbar k_S \hat{a}_S^\dagger(z) \hat{a}_S(z) + \hbar k_A \hat{a}_A^\dagger(z) \hat{a}_A(z) \\ & + \hbar k_V \hat{a}_V^\dagger(z) \hat{a}_V(z) \\ & + \left[ \hbar \tilde{g}_S \hat{a}_V^\dagger(z) \hat{a}_S^\dagger(z) |\alpha_L| \exp(ik_L z + i\phi_L) \right. \\ & \left. + \hbar \tilde{g}_A \hat{a}_V(z) \hat{a}_A^\dagger(z) |\alpha_L| \exp(ik_L z + i\phi_L) + \text{H.c.} \right]. \end{aligned} \quad (1)$$

In Eq. (1), the symbols  $\hat{a}_S$ ,  $\hat{a}_A$  and  $\hat{a}_V$  ( $\hat{a}_S^\dagger$ ,  $\hat{a}_A^\dagger$  and  $\hat{a}_V^\dagger$ ) stand, in turn, for the annihilation (creation) operators

of the Stokes, anti-Stokes and vibrational modes. The nonlinear coupling constant in the Stokes (anti-Stokes) interaction is denoted as  $\tilde{g}_S$  ( $\tilde{g}_A$ ),  $\hbar$  is the reduced Planck constant and H.c. replaces the Hermitian conjugated terms. The law of energy conservation requires the following conditions for the mode frequencies:

$$\omega_S = \omega_L - \omega_V, \quad \omega_A = \omega_L + \omega_V. \quad (2)$$

The correlations between the Stokes and anti-Stokes modes emerge via the interaction with the common vibrational mode whose dynamics plays an important role. For this reason, we describe both its damping and population by thermal phonons. Damping of the vibrational mode originates in its interaction with the reservoir composed of a large number of vibrational modes with frequency  $\omega_V$ , wave vectors  $k_{V,l}$  and linear coupling constants  $\chi_{V,l}$ . Introducing their annihilation (creation) operators  $\hat{a}_{V,l}$  ( $\hat{a}_{V,l}^\dagger$ ), we can write the appropriate interaction momentum operator  $\hat{G}_R(z)$  as follows:

$$\begin{aligned} \hat{G}_R(z) = & \hbar \sum_l k_{V,l} \hat{a}_{V,l}^\dagger(z) \hat{a}_{V,l}(z) \\ & - \hbar \sum_l \left[ \chi_{V,l} \hat{a}_V^\dagger(z) \hat{a}_{V,l}(z) + \text{H.c.} \right]. \end{aligned} \quad (3)$$

Spatial evolution of the optical fields and vibrational modes governed by the overall momentum operator  $\hat{G}(z) + \hat{G}_R(z)$  is described by the Heisenberg equations analogous to those commonly written for the Hamiltonian,  $d\hat{a}(z)/dz = -i/\hbar[\hat{G}(z), \hat{a}(z)]$ . This corresponds to the scheme of field photon-flux quantization [45] suitable also for nonhomogeneous media. We note that this method has been widely applied to study the propagation of nonlinearly interacting optical fields (see [10, 17, 46] and references therein). In our case, the Heisenberg equations corresponding to the momentum operator  $\hat{G}(z) + \hat{G}_R(z)$  take the form:

$$\begin{aligned} \frac{d\hat{a}_S(z)}{dz} &= ik_S \hat{a}_S(z) + g_S \hat{a}_V^\dagger(z) \exp(ik_L z), \\ \frac{d\hat{a}_A(z)}{dz} &= ik_A \hat{a}_A(z) + g_A \hat{a}_V(z) \exp(ik_L z), \\ \frac{d\hat{a}_V(z)}{dz} &= ik_V \hat{a}_V(z) + g_S \hat{a}_S^\dagger(z) \exp(ik_L z) \\ &\quad - g_A^* \hat{a}_A(z) \exp(-ik_L z) - i \sum_l \chi_{V,l} \hat{a}_{V,l}(z), \\ \frac{d\hat{a}_{V,l}(z)}{dz} &= ik_{V,l} \hat{a}_{V,l}(z) - i \chi_{V,l}^* \hat{a}_V(z) \end{aligned} \quad (4)$$

and  $g_{S,A} = i\tilde{g}_{S,A}|\alpha_L| \exp(i\phi_L)$ .

The equations in (4) were derived assuming the following canonical commutation relations among the field operators at arbitrary positions  $z$  and  $z'$  compatible with photon-flux quantization:

$$\begin{aligned} [\hat{a}_b(z), \hat{a}_c(z')] &= 0, \\ [\hat{a}_b(z), \hat{a}_c^\dagger(z')] &= \delta_{bc} \delta(z - z'), \quad b, c = S, A, V; \end{aligned} \quad (5)$$

$\delta_{bc}$  stands for the Kronecker symbol and  $\delta$  means the Dirac function. The commutation relations (5) represent the spatial analog of the usual commutation relations written in time and originating in energy quantization. The quantization of photon flux is compatible with the problems of propagating optical fields as it guarantees the continuity of electric-field amplitude per one quantized photon at the boundaries and as such it can be applied also to field propagation in nonhomogeneous media. The effects of spectral and spatial dispersion important for spatially-localized optical pulses can then be addressed using the spectral and spatial mode decomposition (see, e.g., in [47]). Though the energy and photon-flux quantization schemes are different, they lead to similar quantum effects. This can be understood from the very similar forms of the Heisenberg equations derived for 'unperturbed' monochromatic plane waves in both quantization schemes (formal substitution  $t \rightarrow z/v$  where  $v$  is an average velocity of the propagating fields).

The solution of Eqs. (4) conserves the following quantity composed of photon/phonon numbers:

$$\begin{aligned} N = & \hat{a}_S^\dagger(z) \hat{a}_S(z) - \hat{a}_A^\dagger(z) \hat{a}_A(z) - \hat{a}_V^\dagger(z) \hat{a}_V(z) \\ & - \sum_l \hat{a}_{V,l}^\dagger(z) \hat{a}_{V,l}(z). \end{aligned} \quad (6)$$

The set of Eqs. (4) of linear operator differential equations can be solved following the approach applied in Ref. [48, 49]. Introducing the interaction picture, in which the operator envelopes  $\hat{A}_{S,A,V} = \hat{a}_{S,A,V} \exp(-ik_{S,A,V}z)$  are defined, and assuming the phase matching of the interacting fields ( $k_L - k_V = k_S$ ,  $k_L + k_V = k_A$ ) we write the solution to Eqs. (4) in the form

$$\begin{aligned} \hat{A}_V(z) &= f_1(z) \hat{A}_V(0) + f_{2,S}(z) \hat{A}_S^\dagger(0) - f_{2,A}^*(z) \hat{A}_A(0) \\ &\quad + \sum_l f_{1,l}(z) \hat{A}_{V,l}(0), \\ \hat{A}_S(z) &= f_{2,S}(z) \hat{A}_V^\dagger(0) + f_{3,S}(z) \hat{A}_S(0) + f_{4,S}(z) \hat{A}_A^\dagger(0) \\ &\quad + \sum_l f_{2,l}(z) \hat{A}_{V,l}^\dagger(0), \\ \hat{A}_A(z) &= f_{2,A}(z) \hat{A}_V(0) - f_{4,A}(z) \hat{A}_S^\dagger(0) - f_{3,A}(z) \hat{A}_A(0) \\ &\quad + \sum_l f_{3,l}(z) \hat{A}_{V,l}(0). \end{aligned} \quad (7)$$

The functions introduced in the solution (7) are defined as

$$\begin{aligned} f_1(z) &= \frac{[\Gamma q(z) - \gamma p(z)]h(z)}{\Gamma}, \\ f_{2,b}(z) &= \frac{4ig_b p(z)h(z)}{\Gamma}, \\ f_{3,b}(z) &= \frac{\Gamma|g_b|^2 - |g_{\bar{b}}|^2[\Gamma q(z) + \gamma p(z)]h(z)}{\Gamma\Omega^2}, \\ f_{4,b}(z) &= \frac{g_b g_{\bar{b}} \{\Gamma - [\Gamma q(z) + \gamma p(z)]h(z)\}}{\Gamma\Omega^2}. \end{aligned}$$

$(b, \bar{b}) = (S, A) \text{ or } (b, \bar{b}) = (A, S),$

$$\begin{aligned}
f_{1,l}(z) &= -i(\chi_{V,l}/\Gamma)\{\Delta k_{V,l}[\Gamma g_l(z) - [\Gamma q(z) - \gamma p(z)]h(z)] \\
&\quad + 4i\Omega^2 p(z)h(z)\} [\Delta k_{V,l}(\gamma - i\Delta k_{V,l}) + i\Omega^2]^{-1}, \\
f_{2,l}(z) &= ig_S(\chi_{V,l}^*/\Gamma)\{\Gamma g_l(z) - [4i\Delta k_{V,l}p(z) + [\Gamma q(z) \\
&\quad + \gamma p(z)]]h(z)\} [\Delta k_{V,l}(\gamma/2 + i\Delta k_{V,l}) - i\Omega^2]^{-1}, \\
f_{3,l}(z) &= ig_A(\chi_{V,l}/\Gamma)\{\Gamma g_l(z) + [4i\Delta k_{V,l}p(z) - [\Gamma q(z) \\
&\quad + \gamma p(z)]]h(z)\} [\Delta k_{V,l}(\gamma/2 - i\Delta k_{V,l}) + i\Omega^2]^{-1}.
\end{aligned} \tag{8}$$

In Eqs. (8), we use functions  $g_l(z) = \exp(i\Delta k_{V,l}z)$ ,  $h(z) = \exp(-\gamma z/4)$ ,  $p(z) = \sinh(\Gamma z/4)$ ,  $q(z) = \cosh(\Gamma z/4)$  and constants  $\Omega = \sqrt{|g_A|^2 - |g_S|^2}$ ,  $\Gamma = \sqrt{\gamma^2 - 16\Omega^2}$  and  $\Delta k_{V,l} = k_{V,l} - k_V$ . The damping constant  $\gamma$  is given, according to the Wigner-Weisskopf theory [14], as  $\gamma = 2\pi|\chi_V|^2 \varrho_V$ , where  $\chi_V$  is an average reservoir coupling constant and  $\varrho_V$  stands for the density of vibrational reservoir modes. We note that the functions defined in Eqs. (8) obey several relations that originate in the bosonic commutation relations at an arbitrary position  $z$ . This is so due to the rigorous description of the vibrational reservoir that causes damping of the vibrational mode and that also acts on the vibrational mode via the corresponding fluctuating operator forces that compensate for damping in the quantum evolution (fluctuation-dissipation theorem).

In our analysis, we assume that the Stokes and anti-Stokes modes are initially in the vacuum states, whereas the vibrational mode and its reservoir vibrational modes are initially in thermal states with the average phonon numbers  $\langle \hat{n}_V(0) \rangle = n_V$  and  $\langle \hat{n}_{V,l} \rangle = n_T$ , respectively. The normal characteristic function  $C_N(\beta_S, \beta_A; z)$ , which is a commonly used tool to access all useful physical quantities (see Sec. III below), encompasses the combined Stokes and anti-Stokes modes and it is defined as

$$\begin{aligned}
C_N(\beta_S, \beta_A; z) &= \langle \exp[\beta_S \hat{A}_S^\dagger(z) + \beta_A \hat{A}_A^\dagger(z)] \\
&\quad \times \exp[-\beta_S^* \hat{A}_S(z) - \beta_A^* \hat{A}_A(z)] \rangle.
\end{aligned} \tag{9}$$

It takes the following Gaussian form for the solution written in Eqs. (7) [14, 46]:

$$\begin{aligned}
C_N(\beta_S, \beta_A; z) &= \exp[-B_S(z)|\beta_S|^2 - B_A(z)|\beta_A|^2] \\
&\quad \times \exp[D_{SA}(z)\beta_S^* \beta_A + \text{c.c.}]
\end{aligned} \tag{10}$$

and symbol c.c. replaces the complex conjugated term.

In Eq. (10), the  $z$ -dependent coefficients are obtained as follows:

$$\begin{aligned}
B_S(z) &= b_S(z, z), \\
b_S(z, z') &= \langle \hat{A}_S^\dagger(z) \hat{A}_S(z') \rangle = f_{2,S}^*(z) f_{2,S}(z') (n_V + 1) \\
&\quad + f_{4,S}^*(z) f_{4,S}(z') + \sum_l f_{2,l}^*(z) f_{2,l}(z') (n_T + 1), \\
B_A(z) &= b_A(z, z), \\
b_A(z, z') &= \langle \hat{A}_A^\dagger(z) \hat{A}_A(z') \rangle = f_{2,A}^*(z) f_{2,A}(z') n_V \\
&\quad + f_{4,A}^*(z) f_{4,A}(z') + \sum_l f_{3,l}^*(z) f_{3,l}(z') n_T,
\end{aligned}$$

$$\begin{aligned}
D_{SA}(z) &= d_{SA}(z, z), \\
d_{SA}(z, z') &= \langle \hat{A}_S(z) \hat{A}_A(z') \rangle = f_{2,S}(z) f_{2,A}(z') n_V \\
&\quad - f_{3,S}(z) f_{4,A}(z') + \sum_l f_{2,l}(z) f_{3,l}(z') n_T.
\end{aligned} \tag{11}$$

The terms on the right-hand sides of Eqs. (11) involving the sum over the vibrational reservoir modes can conveniently be determined from the commutation relations  $[\hat{A}_S(z), \hat{A}_S^\dagger(z)] = 1$ ,  $[\hat{A}_A(z), \hat{A}_A^\dagger(z)] = 1$ , and  $[\hat{A}_S(z), \hat{A}_A(z)] = 0$  provided that  $z = z'$ . In turn, they give us:

$$\begin{aligned}
\sum_l |f_{2,l}(z)|^2 &= -1 - |f_{2,S}(z)|^2 + |f_{3,S}(z)|^2 - |f_{4,S}(z)|^2, \\
\sum_l |f_{3,l}(z)|^2 &= 1 - |f_{2,A}(z)|^2 - |f_{3,A}(z)|^2 + |f_{4,A}(z)|^2, \\
\sum_l f_{2,l}(z) f_{3,l}(z) &= -f_{2,S}(z) f_{2,A}(z) - f_{3,S}(z) f_{4,A}(z) \\
&\quad + f_{4,S}(z) f_{3,A}(z).
\end{aligned} \tag{12}$$

### III. QUANTIFICATION OF CORRELATIONS BETWEEN THE STOKES AND ANTI-STOKES FIELDS

Owing to the relationship between the Stokes and anti-Stokes modes mediated by the vibrational mode the correlations between the Stokes and anti-Stokes modes are developing as the Raman process proceeds. These correlations manifest themselves in various ways starting from the usual classical intensity correlations and ending with the steering and the Bell nonlocality between the modes that expresses the exclusively quantum influence of one mode to the other mode.

The coherence theory defines the normalized intensity cross-correlation function  $g_{SA}^{(2)}(z, z')$  between the Stokes intensity at position  $z$  and anti-Stokes intensity at position  $z'$  [14, 50],

$$g_{SA}^{(2)}(z, z') = \frac{\langle \hat{A}_S^\dagger(z) \hat{A}_A^\dagger(z') \hat{A}_A(z') \hat{A}_S(z) \rangle}{\langle \hat{A}_S^\dagger(z) \hat{A}_S(z) \rangle \langle \hat{A}_A^\dagger(z') \hat{A}_A(z') \rangle}, \tag{13}$$

to quantify the mutual relation between the Stokes and anti-Stokes fields. Whereas the mean photon numbers  $\langle \hat{A}_S^\dagger \hat{A}_S \rangle$  and  $\langle \hat{A}_A^\dagger \hat{A}_A \rangle$  in Eq. (13) are given by the coefficients  $B_S$  and  $B_A$  in Eqs. (11), respectively, the remaining fourth order amplitude correlation function is determined as follows:

$$\begin{aligned}
&\langle \hat{A}_S^\dagger(z) \hat{A}_A^\dagger(z') \hat{A}_A(z') \hat{A}_S(z) \rangle \\
&= B_S(z) B_A(z') + |d_{SA}(z, z')|^2.
\end{aligned} \tag{14}$$

The  $g^{(2)}$  function defined in Eq. (13) identifies possible bunching of photons residing in two modes.

Nonclassical character of two-mode fields is often tested by the violation of the Cauchy-Schwarz inequality that represents one of the simplest and also most powerful nonclassicality witnesses [50]:

$$\begin{aligned}
&\langle \hat{A}_S^\dagger(z) \hat{A}_A^\dagger(z) \hat{A}_A(z) \hat{A}_S(z) \rangle^2 \leq \\
&\langle \hat{A}_S^{\dagger 2}(z) \hat{A}_S^2(z) \rangle \langle \hat{A}_A^{\dagger 2}(z) \hat{A}_A^2(z) \rangle.
\end{aligned} \tag{15}$$



As the Stokes and anti-Stokes modes evolve from the vacuum states, their statistics remain chaotic and so we have  $\langle \hat{A}_b^{\dagger 2}(z) \hat{A}_b^2(z) \rangle = 2[\langle \hat{A}_b^{\dagger}(z) \hat{A}_b(z) \rangle]^2$ ,  $b = S, A$ . Under these conditions, the Cauchy-Schwarz inequality (15) is transformed into the following non-classicality inequality:

$$g_{SA}^{(2)}(z) > 2. \quad (16)$$

Correlations in photon numbers  $\hat{n}_S \equiv \hat{a}_S^{\dagger} \hat{a}_S = \hat{A}_S^{\dagger} \hat{A}_S$  and  $\hat{n}_A \equiv \hat{a}_A^{\dagger} \hat{a}_A = \hat{A}_A^{\dagger} \hat{A}_A$  of the Stokes and anti-Stokes fields, respectively, are characterized by the noise-reduction-factor  $R_{SA}$  [10]:

$$R_{SA}(z) = \frac{\langle (\Delta[\hat{n}_S(z) - \hat{n}_A(z)])^2 \rangle}{\langle \hat{n}_S(z) \rangle + \langle \hat{n}_A(z) \rangle}; \quad (17)$$

$\Delta \hat{x} = \hat{x} - \langle \hat{x} \rangle$  gives the fluctuation of operator  $\hat{x}$ . The values of  $R_{SA}$  smaller than one are reserved for nonclassical fields for which the fluctuations of the difference of the Stokes and anti-Stokes photon numbers are suppressed below the quantum Poissonian limit. In the limiting case of  $R_{SA} = 0$ , the Stokes and anti-Stokes fields can be considered as composed of only photon pairs having one photon in the Stokes mode and the accompanying photon in the anti-Stokes mode. This case represents the most non-classical two-mode fields. Individual photons comprising a photon pair are in this case completely indistinguishable (apart from different frequencies). Provided that the difference in the Stokes and anti-Stokes field frequencies is omitted, the photons give visibility one in the Hong-Ou-Mandel interferometer [51], i.e., they coalesce at a beam splitter. The fraction of paired photons in the two-mode field can roughly be estimated as  $1 - R_{SA}$ . Using the coefficients in Eqs. (11), the noise-reduction-factor  $R_{SA}$  is expressed as:

$$R_{SA}(z) = 1 + \frac{B_S^2(z) + B_A^2(z) - 2|D_{SA}(z)|^2}{B_S(z) + B_A(z)}. \quad (18)$$

The Stokes and anti-Stokes fields can also exhibit non-classical correlations in their phase properties. The strength of such correlations is described by the two-mode principal squeezing variance  $\lambda_{SA}$  [52] that is determined by the following formula [17]:

$$\lambda_{SA}(z) = 1 + B_S(z) + B_A(z) - 2|D_{SA}(z)|. \quad (19)$$

We have  $0 < \lambda_{SA} < 1$  for nonclassical fields. The smaller the value of  $\lambda_{SA}$  is the stronger the quantum phase correlations are and the more reduced the fluctuations of the relative phase below the quantum limit given by the Heisenberg uncertainty relations are.

In general, we can quantify the entanglement of the Stokes and anti-Stokes fields by determining the logarithmic negativity [53]. It is derived from the covariance matrix [54],

$$\sigma(z) = \begin{bmatrix} \sigma_S(z) & \sigma_{SA}(z) \\ \sigma_{SA}(z) & \sigma_A(z) \end{bmatrix}, \quad (20)$$

$$\sigma_b(z) = \begin{bmatrix} 1 + 2B_b(z) & 0 \\ 0 & 1 + 2B_b(z) \end{bmatrix}, \quad b = S, A, \\ \sigma_{SA}(z) = 2 \begin{bmatrix} \text{Re}\{D_{SA}(z)\} & -i\text{Im}\{D_{SA}(z)\} \\ -i\text{Im}\{D_{SA}(z)\} & -\text{Re}\{D_{SA}(z)\} \end{bmatrix}. \quad (21)$$

The symplectic eigenvalues  $\xi_{\pm}$  of the partially-transposed covariance matrix  $\sigma$  [55, 56] attain the form

$$2\xi_{\pm}^2(z) = \sum_{b=S,A} [1 + 2B_b(z)]^2 + 8\text{Re}\{D_{SA}^2(z)\} \\ + 4[1 + B_S(z) + B_A(z)] \\ \times \sqrt{[B_S(z) - B_A(z)]^2 + 4\text{Re}\{D_{SA}^2(z)\}}. \quad (22)$$

Symbol  $\text{Re}$  ( $\text{Im}$ ) denotes the real (imaginary) part of an expression. If  $\xi_- < 1$  we arrive at the nonzero logarithmic negativity  $E_{\mathcal{N},SA}$  along the formula

$$E_{\mathcal{N},SA}(z) = -\ln[\xi_-(z)], \quad (23)$$

where  $\ln$  stands for the natural logarithm. The entangled states have  $E_{\mathcal{N}} > 0$ : The greater the logarithmic negativity  $E_{\mathcal{N}}$  is, the more entangled the state is and the more quantum the state properties are.

We note that the entropy cannot be applied to quantify the entanglement as the common state of the Stokes and anti-Stokes fields is in general mixed. Purity  $\mu_{SA}(z)$  that measures the mixedness of a state is determined as

$$\mu_{SA}(z) = 1/\sqrt{\det[\sigma(z)]} \\ = 1/[ [1 + 2B_S(z)][1 + 2B_A(z)] - 4\text{Re}\{D_{SA}^2(z)\} ] \quad (24)$$

where  $\det$  denotes the determinant of a matrix. The smaller the purity is the more complex the internal structure of the state is.

Alternatively, as the reduced states of the Stokes and anti-Stokes modes are chaotic, i.e. classical, the Lee non-classicality depth  $\tau_{SA}$  [57] can be applied to quantify the entanglement between the Stokes and anti-Stokes fields. It gives the amount of the noise needed to conceal the non-classicality of the analyzed field. For the considered two-mode field, the non-classicality depth  $\tau_{SA}$  is determined as follows [58]:

$$\tau_{SA}(z) = \max\{0, -[B_S(z) + B_A(z)]/2 \\ + \sqrt{[B_S(z) - B_A(z)]^2 + 4|D_{SA}(z)|^2}/2\}. \quad (25)$$

For two-mode Gaussian states,  $\tau_{SA} \leq 1/2$  and the greater the non-classicality depth  $\tau_{SA}$  is, the more nonclassical the state is.

Owing to the microscopic origin of the correlations, in which the Stokes and anti-Stokes modes play different roles, the correlations between the modes are asymmetric. To quantify this asymmetry, we use the steering parameter  $\mathcal{S}_{b \rightarrow c}$  [59] that tells us to which extent we can steer the state of subsystem  $c$  by the measurement on the state of subsystem  $b$ . We have for two-mode Gaussian states and Gaussian measurements on the state of

subsystem  $b$  [60]:

$$\mathcal{S}_{b \rightarrow c}(z) = \max \{0, \ln(\det[\sigma_b(z)] / \det[\sigma(z)]) / 2\},$$

$$(b, c) = (S, A) \text{ or } (A, S). \quad (26)$$

The Stokes and anti-Stokes fields are not only entangled, they may even exhibit the Bell-type correlations — the strongest quantum correlations. The corresponding hidden-variable model [61, 62] is constructed upon the joint displaced parity operator

$$\hat{\Pi}(\beta_S, \beta_A) = \hat{D}_S(\beta_S)(-1)^{\hat{A}_S^\dagger \hat{A}_S} \hat{D}_S^\dagger(\beta_S) \\ \otimes \hat{D}_A(\beta_A)(-1)^{\hat{A}_A^\dagger \hat{A}_A} \hat{D}_A^\dagger(\beta_A), \quad (27)$$

where the symbol  $\hat{D}_b(\beta_b)$  denotes the displacement operator in mode  $b$  [ $\hat{D}_b(\beta_b) = \exp(\beta_b \hat{A}_b^\dagger - \text{H.c.})$ ]. The mean value  $\Pi(\beta_S, \beta_A)$  of the operator  $\hat{\Pi}(\beta_S, \beta_A)$  can easily be obtained owing to its relation to the Wigner function  $W$ ,

$$\Pi(\beta_S, \beta_A) = \frac{\pi^2}{4} W(\beta_S, \beta_A). \quad (28)$$

The Wigner function is then determined by the Fourier transform of the symmetrically-ordered characteristic function  $\mathcal{C}_S(\beta_S, \beta_A)$  that is derived from its normally-ordered form  $\mathcal{C}_N(\beta_S, \beta_A)$  in Eq. (10) by the replacement  $B_S \leftarrow B_S + 1/2$  and  $B_A \leftarrow B_A + 1/2$ . As the parity operator is a dichotomic variable, it may be used to define the Bell-like inequalities [63]. The corresponding Bell parameter is then defined as follows using the mean values of suitably chosen displaced parity operators [61]:

$$\mathcal{B}_{SA}(\beta_{S1}, \beta_{S2}, \beta_{A1}, \beta_{A2}) = \Pi(\beta_{S1}, \beta_{A1}) + \Pi(\beta_{S2}, \beta_{A1}) \\ + \Pi(\beta_{S1}, \beta_{A2}) - \Pi(\beta_{S2}, \beta_{A2}). \quad (29)$$

If, for any suitably chosen set of parameters  $\beta_{S1}$ ,  $\beta_{S2}$ ,  $\beta_{A1}$  and  $\beta_{A2}$ , the Bell parameter  $\mathcal{B}_{SA}$  exceeds two, any hidden-variable theory cannot be considered and we speak about the nonlocal Bell-type correlations.

#### IV. THE RAMAN PROCESS WITH AN IDEAL VIBRATIONAL MODE IN THE INITIAL VACUUM STATE

The strongest correlation between the Stokes and anti-Stokes fields is expected provided that the vibrational mode is initially in the vacuum state and is not damped. In this case, there has to exist a Stokes photon for each anti-Stokes photon because creation of an anti-Stokes photon in the anti-Stokes interaction is accompanied by annihilation of a vibrational phonon that was created in the Stokes interaction together with the Stokes photon. Additional thermal phonons, that exist independently of the Stokes interaction, make the anti-Stokes interaction independent of the Stokes field and thus weaken the correlations between the Stokes and anti-Stokes modes. Similarly, damping of the vibrational mode, that removes the phonons comprising pairs with the Stokes photons

and also adds independent phonons, partially breaks the correlations between the Stokes and vibrational modes and thus weakens the correlations between the Stokes and anti-Stokes modes.

In this ideal case, crucial role in forming the correlations is played by the ratio  $\epsilon$  of the squared moduli of anti-Stokes and Stokes nonlinear coupling constants,  $\epsilon = |g_A|^2 / |g_S|^2$ . The ratio  $\epsilon$  is a characteristic parameter of the medium exhibiting the Raman process [64]. In the analysis of the solution (7), we assume that the phase  $\phi_L$  of the laser pump beam is such that the nonlinear coupling constants  $g_S$  and  $g_A$  are real and positive ( $\phi_L = -\pi/2$ ) which maximizes the quantum correlations in the Raman process. We note that the coupling constants  $\tilde{g}_S$  and  $\tilde{g}_A$  involved in Eq. (1) are real and positive as they quantify the corresponding coupling momentum (energy). Then we identify two different regimes in the dynamics of the Raman process as described by the solution (7): The intensities of the Stokes and anti-Stokes modes exponentially increase for  $\epsilon \leq 1$ , whereas they show periodic solution for  $\epsilon > 1$ .

The validity of the exponential solution is limited by the assumption of un-depleted pump field that allows the transfer of just a small fraction of the pump energy into the Stokes and anti-Stokes fields. On the other hand, the periodic solution originates in the competition of the Stokes and anti-Stokes interactions for the vibrational phonons and such interactions are known to behave as if they are phase-mismatched [46]: The greater the ratio  $\epsilon > 1$  is, the greater the effective phase-mismatch is and so the smaller the fraction of the pump energy accessible for the transfer into the Stokes and anti-Stokes fields [13]. Experimental investigations of the Raman process under the condition  $\epsilon > 1$  can be found, e.g., in Refs. [65, 66]. We note that some aspects of pump depletion in quantum models of the Raman process were discussed, e.g., in Refs. [14, 67].

Straightforward calculations in the case  $\epsilon \leq 1$  leave us with the following coefficients in the characteristic function  $\mathcal{C}_N(\beta_S, \beta_A; z)$  in Eq. (10):

$$B_A^{\text{id,e}}(z) = 4\epsilon \sinh^4(g_S z \sqrt{1 - \epsilon}/2) / (1 - \epsilon)^2, \\ B_S^{\text{id,e}}(z) = B_A^{\text{id,e}}(z) + \sinh^2(g_S z \sqrt{1 - \epsilon}) / (1 - \epsilon), \\ D_{SA}^{\text{id,e}}(z) = \sqrt{\epsilon} [\epsilon - \cosh(g_S z \sqrt{1 - \epsilon})] \\ \times [\cosh(g_S z \sqrt{1 - \epsilon}) - 1] / (1 - \epsilon)^2. \quad (30)$$

On the other hand, the coefficients of the characteristic function  $\mathcal{C}_N$  for the periodic solution valid for  $\epsilon > 1$  are written as:

$$B_A^{\text{id,p}}(z) = 4\epsilon \sin^4(g_S z \sqrt{\epsilon - 1}/2) / (\epsilon - 1)^2, \\ B_S^{\text{id,p}}(z) = B_A^{\text{id,p}}(z) + \sin^2(g_S z \sqrt{\epsilon - 1}) / (\epsilon - 1), \\ D_{SA}^{\text{id,p}}(z) = \sqrt{\epsilon} [\epsilon - \cos(g_S z \sqrt{\epsilon - 1})] \\ \times [\cos(g_S z \sqrt{\epsilon - 1}) - 1] / (\epsilon - 1)^2. \quad (31)$$

An important characteristic of the coefficients in Eqs. (30) and (31), that give the fields properties, is that

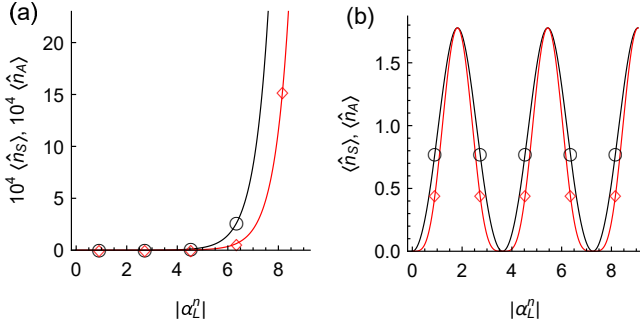


FIG. 2. (a,b) Stokes [anti-Stokes] mean photon number  $\langle \hat{n}_S \rangle$  [ $\langle \hat{n}_A \rangle$ ] ( $\circ$ ) [(red  $\diamond$ )] in exponential (a) and oscillatory (b) regimes. The used parameters are:  $\epsilon = 1/4$  ( $\epsilon = 4$ ) in exponential (oscillatory) regime,  $\gamma^n = 0$ ,  $n_V = n_T = 0$ .

they depend on the product of the Stokes nonlinear coupling constant  $\tilde{g}_S$ , the pump-beam amplitude  $|\alpha_L|$  and the interaction length  $z$ . For this reason, we further discuss the fields properties as they depend on the 'cumulative' normalized nonlinear pump amplitude  $|\alpha_L^n|$  defined for a Raman medium of length  $L$ :

$$|\alpha_L^n| \equiv \tilde{g}_S |\alpha_L| L. \quad (32)$$

We also introduce the normalized damping constant  $\gamma^n \equiv \gamma L$ .

The conservation law in Eq. (6) for mean photon/phonon numbers guarantees that the number  $\langle \hat{n}_A \rangle^{\text{id}}$  of anti-Stokes photons cannot exceed the number  $\langle \hat{n}_S \rangle^{\text{id}}$  of Stokes photons. Whereas the difference  $\langle \hat{n}_S \rangle^{\text{id}} - \langle \hat{n}_A \rangle^{\text{id}}$  of these photon numbers, that in fact gives the number  $\langle \hat{n}_V \rangle^{\text{id}}$  of vibrational phonons, monotonously increases with the increasing pump amplitude  $|\alpha_L^n|$  in the exponential regime [see Fig. 2(a)], it equals to zero for specific values of the pump amplitude  $|\alpha_L^n|$  in the oscillatory regime [see Fig. 2(b)]. For these pump amplitudes numbered by  $m$ , the Stokes and anti-Stokes photon numbers coincide [ $\langle \hat{n}_S \rangle^{\text{id}}(|\alpha_{L,m}^n|) = \langle \hat{n}_A \rangle^{\text{id}}(|\alpha_{L,m}^n|)$ ] and moreover the vibrational mode is in the vacuum state [ $\langle \hat{n}_V \rangle^{\text{id}}(|\alpha_{L,m}^n|) = 0$ ].

In both the exponential and oscillatory regimes, the  $g_{SA}^{(2)}$  intensity function decreases from high nonclassical values with the increasing pump amplitude  $|\alpha_L^n|$  [see Fig. 3(a)]. This decrease is exponential in the exponential regime and ends up at the classical value  $g_{SA}^{(2)} = 2$ . In the oscillatory regime, it stops at the pump amplitude  $|\alpha_{L,1}^n| = \pi/\sqrt{\epsilon-1}$  at which the Stokes and anti-Stokes photon numbers coincide and reach their maximal values. Then, according to the formulas in Eqs. (31) the dependence  $g_{SA}^{(2)}(|\alpha_L^n|)$  is periodic and the attained values are nonclassical for all pump amplitudes. Qualitative difference in the fields evolution in both regimes is clearly documented by the values of the purity  $\mu_{SA}$ . Whereas the purity  $\mu_{SA}$  monotonously decreases from the initial value  $\mu_{SA} = 1$  of the pure vacuum state with the increasing pump amplitude  $|\alpha_L^n|$  in the exponential regime

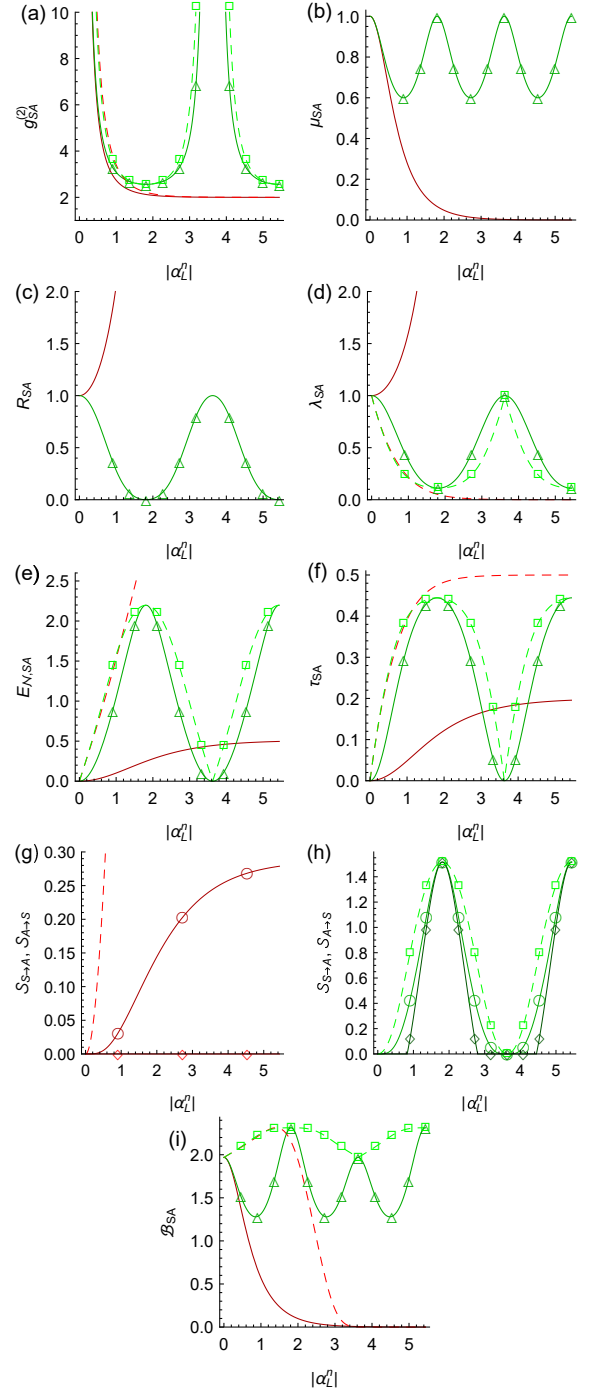


FIG. 3. (a)  $g_{SA}^{(2)}$  intensity function, (b) purity  $\mu_{SA}$ , (c) noise-reduction-factor  $R_{SA}$ , (d) principal squeezing variance  $\lambda_{SA}$ , (e) logarithmic negativity  $E_{N,SA}$ , (f) non-classicality depth  $\tau_{SA}$ , (g,h) steering parameter  $\mathcal{S}_{S \rightarrow A}$  [ $\mathcal{S}_{A \rightarrow S}$ ] ( $\circ$ ) [( $\diamond$ )] in exponential (g) and oscillatory (h) regimes and (i) the Bell parameter  $\mathcal{B}_{SA}$  as they depend on normalized pump amplitude  $|\alpha_L^n|$ . In (a)–(f) and (i), curves for exponential (dark red plain solid curve) and oscillatory (green plain solid curves with  $\triangle$ ) regimes are plotted. In (a)–(i), the light red plain dashed curves and the light green dashed curves with  $\square$  characterize parametric down-conversion with mean signal/idler photon number  $\langle \hat{n}_{\text{spdc}} \rangle = (\langle \hat{n}_S \rangle + \langle \hat{n}_A \rangle)/2$  in the exponential and oscillatory regimes, respectively (for details, see Appendix A). The used parameters are given in the caption to Fig. 2.

[see Fig. 3(b)], it behaves periodically in the oscillatory regime. This means that the fields purity  $\mu_{SA}$  initially decreases with the increasing pump amplitude  $|\alpha_L^n|$  but then it starts to increase and the fields state is pure at the pump amplitude  $|\alpha_{L,1}^n|$ .

In the exponential regime, nonclassical correlations in the Stokes and anti-Stokes modes as identified by the noise-reduction-factor  $R_{SA}$  are not built [see Fig. 3(c)]. On the other hand, they exist in the oscillatory regime for any pump amplitude  $|\alpha_L^n|$  and even reach their maximal nonclassical value ( $R_{SA} = 0$ ) for the pump amplitude  $|\alpha_{L,1}^n|$ . The correlations in the phases of the Stokes and anti-Stokes fields as quantified by the two-mode principal squeezing variance  $\lambda_{SA}$  behave similarly [see Fig. 3(d)]. Nevertheless, the fields entanglement in the exponential regime develops and it becomes stronger with the increasing pump amplitude  $|\alpha_L^n|$ . The increase of the entanglement with the increasing pump amplitude  $|\alpha_L^n|$  is quantified by the logarithmic negativity  $E_{N,SA}$  [see Fig. 3(e)] and the non-classicality depth  $\tau_{SA}$  [see Fig. 3(f)]. Whereas the logarithmic negativity  $E_{N,SA}$  directly quantifies the entanglement, the asymptotic value of the non-classicality  $\tau_{SA} = 1/2$  reached for  $|\alpha_L^n| \rightarrow \infty$  identifies the asymptotic state as the most nonclassical among all two-mode Gaussian states. The values of the logarithmic negativity  $E_{N,SA}$  and the non-classicality depth  $\tau_{SA}$  attained in the oscillatory regime, that are maximal for the pump amplitude  $|\alpha_{L,1}^n|$ , are smaller than the asymptotic values reached in the exponential regime. This occurs despite the fact that the Stokes and anti-Stokes photons are perfectly paired for  $|\alpha_{L,1}^n|$  and it is caused by smaller fields intensities in the oscillatory regime.

Steering shows asymmetry in both regimes [see Fig. 3(g,h)]. Owing to the microscopic mechanism of the Raman process, steering of the anti-Stokes mode by the Stokes mode is more efficient than the opposed case. The only exception occurs in the oscillatory regime for  $|\alpha_{L,1}^n|$  where the Stokes and anti-Stokes field properties are identical and the steering is symmetric. Similarly as in case of the entanglement measures, the steering parameters  $\mathcal{S}_{S \rightarrow A}$  and  $\mathcal{S}_{A \rightarrow S}$  attain larger values in the exponential regime as a consequence of greater fields intensities for sufficiently high pump amplitudes not shown in Fig. 3(g,h). Whereas the states exhibiting the nonlocal Bell correlations ( $\mathcal{B}_{SA} > 2$ ) are observed in the periodic regime for the pump amplitudes around  $|\alpha_{L,m}^n|$ ,  $m = 1, 2, \dots$  [see Fig. 3(i)], the Bell correlations cannot be obtained in the exponential regime. To get the curves in Fig. 3(i) [and also Fig. 6(i) below], we have numerically optimized the parameters of the Bell measurement [ $\beta_{S1} = -\beta_{A1} = i\sqrt{\mathcal{J}}$ ,  $\mathcal{J} = 3.5 \times 10^{-3}$ ,  $\beta_{S2} = -\beta_{A2} = -q\beta_{S1}$ ,  $q = 3.09$ , for the symbols, see Eq. (37) below] to reach the Bell parameter  $\mathcal{B}_{\max} = 2.313$ . We note that the phases of the optimized complex parameters differ from those appropriate for parametric down-conversion to compensate for the negative sign of the coefficient  $D_{SA}$ .

According to the above discussion, optimal conditions for pairing of the Stokes and anti-Stokes photons are found in the oscillatory regime for the pump amplitudes  $|\alpha_{L,m}^n| = (2m - 1)\pi/\sqrt{\epsilon - 1}$ ,  $m = 1, 2, \dots$ . At these  $|\alpha_{L,m}^n|$ , the mean numbers of Stokes and anti-Stokes photons coincide and they solely depend on the ratio  $\epsilon$ :

$$\langle \hat{n}_S \rangle^{\text{id},m} = \langle \hat{n}_A \rangle^{\text{id},m} = 4\epsilon/(\epsilon - 1)^2. \quad (33)$$

We also have  $D_{SA}^{\text{id},m} = -2\sqrt{\epsilon}(\epsilon + 1)/(\epsilon - 1)^2$ . Both the mean photon numbers  $\langle \hat{n}_S \rangle^{\text{id},m}$  and  $\langle \hat{n}_A \rangle^{\text{id},m}$  as well as the modulus of coefficient  $D_{SA}^{\text{id},m}$  decrease with the increasing ratio  $\epsilon$ . Physically, this means that the increasing strength of the nonlinear anti-Stokes interaction relative to the Stokes one, that makes the population oscillations in the anti-Stokes interaction faster, effectively decouples the anti-Stokes mode and, moreover, disturbs the Stokes interaction. We note that for the pump amplitudes  $|\alpha_{L,m}^n| = 2m\pi/\sqrt{\epsilon - 1}$  and  $m = 1, \dots$  the Stokes and anti-Stokes modes (as well as the vibrational mode) return to the initial vacuum states.

Returning back to the condition  $\langle \hat{n}_S \rangle^{\text{id},m} = \langle \hat{n}_A \rangle^{\text{id},m}$ , the conservation law of photon/phonon numbers gives the mean phonon number  $\langle \hat{n}_V \rangle^{\text{id},m}$  equal to zero, i.e., the vibrational mode is in the vacuum state and the common state of the Stokes and anti-Stokes modes is pure. We also have  $|D_{SA}^{\text{id},m}|^2 = B_S^{\text{id},m}[B_S^{\text{id},m} + 1]$ . This relation for the coefficients in the normal characteristic function  $C_N$  is well known from parametric down-conversion, in which it describes ideal twin beams with perfect correlations in the signal and idler photon numbers [for details, see Appendix A]. However, the coefficient  $D_{SA}^{\text{id},m}$  has the negative sign contrary to the case of parametric down-conversion. This means, that, on average, the positive fluctuation  $\Delta \hat{A}_S$  of the Stokes-field amplitude is accompanied by the negative fluctuation  $\Delta \hat{A}_A$  of the anti-Stokes-field amplitude. This behavior originates in the form of the anti-Stokes interaction in which the creation of a phonon is accompanied by the annihilation of an anti-Stokes photon. In analogy to the state generated in parametric down-conversion [11], the common state of the Stokes and anti-Stokes fields is written as (for details, see Appendix B):

$$|\psi\rangle_{SA}^{\text{id}} = \sum_{n_S, n_A=0}^{\infty} (-1)^{n_S} \sqrt{p_{SA}^{\text{id}}(n_S, n_A)} |n_S\rangle_S |n_A\rangle_A, \\ p_{SA}^{\text{id}}(n_S, n_A) = \delta_{n_S, n_A} B^{n_S} / (1 + B)^{1+n_S}, \quad (34)$$

where  $|n_S\rangle_S$  ( $|n_A\rangle_A$ ) means the Fock state with  $n_S$  ( $n_A$ ) Stokes (anti-Stokes) photons,  $p_{SA}^{\text{id}}(n_S, n_A)$  stands for the joint Stokes–anti-Stokes photon-number distribution and  $B$  gives the mean number of photon pairs.

More generally, the joint Stokes–anti-Stokes photon-number distribution  $p_{SA}^{\text{id}}$  has nonzero probabilities only for  $n_S \geq n_A$  provided that  $n_V = 0$  [68]:

$$p_{SA}^{\text{id}}(n_S, n_A) = \binom{n_S}{n_A} \frac{(B_A^{\text{id}})^{n_A} (B_S^{\text{id}} - B_A^{\text{id}})^{n_S - n_A}}{(1 + B_S^{\text{id}})^{1+n_S}},$$



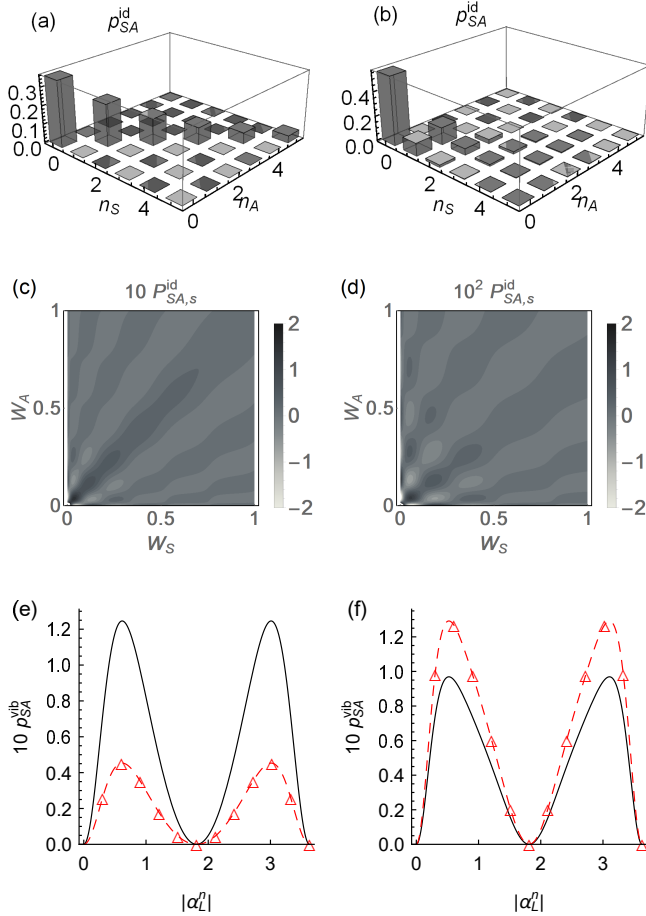


FIG. 4. (a,b) Joint Stokes and anti-Stokes photon-number distribution  $p_{SA}^{\text{id}}(n_S, n_A)$  and (c,d) the corresponding quasi-distribution  $P_{SA,s}^{\text{id}}(W_S, W_A)$  of integrated intensities for (a,c)  $s = 0.12$  and pump amplitude  $|\alpha_{L,1}^n|$  and (b,d)  $s = 0.45$  and  $|\alpha_{L,1}^n|/2$ ;  $\epsilon = 4$ ,  $\gamma^n = 0$ ,  $n_V = n_T = 0$ . In (e) and (f), probabilities  $p_{SA}^{\text{vib}}(1, 0)$  [black plain curves] and  $p_{SA}^{\text{vib}}(0, 1)$  [red curves with  $\triangle$ ] are plotted assuming  $n_V = 0.1$  (e) and  $n_V = 0.5$  (f).

$$n_S \geq n_A. \quad (35)$$

The ideally-paired joint photon-number distribution  $p_{SA}^{\text{id}}$  is compared with the more general one in Eq. (35) in Figs. 3(a,b).

The  $s$ -ordered quasi-distribution  $P_{SA,s}^{\text{id}}$  of integrated Stokes ( $W_S$ ) and anti-Stokes ( $W_A$ ) intensities belonging to the photon-number distribution  $p_{SA}^{\text{id}}$  and determined along the formula [68]

$$\begin{aligned} P_{SA,s}^{\text{id}}(W_S, W_A) &= \frac{4}{(1-s)^2} \exp\left(-\frac{2(W_S + W_A)}{1-s}\right) \\ &\times \sum_{n_S, n_A=0}^{\infty} \frac{p_{SA}^{\text{id}}(n_S, n_A)}{n_S! n_A!} \left(\frac{s+1}{s-1}\right)^{n_S+n_A} \\ &\times L_{n_S}\left(\frac{4W_S}{1-s^2}\right) L_{n_A}\left(\frac{4W_A}{1-s^2}\right) \end{aligned} \quad (36)$$

documents the nonclassical character of the analyzed

fields via its negative values. In Eq. (36), the symbol  $L_k$  stands for the Laguerre polynomials [69]. To demonstrate the properties of the  $s$ -ordered quasi-distributions  $P_{SA,s}^{\text{id}}$ , we have determined them for the balanced [ $\langle \hat{n}_S \rangle = \langle \hat{n}_A \rangle$ ], for the joint Stokes–anti-Stokes photon-number distribution  $p_{SA}^{\text{id}}$ , see Fig. 4(a)] as well as un-balanced [ $\langle \hat{n}_S \rangle \neq \langle \hat{n}_A \rangle$ ], for  $p_{SA}^{\text{id}}$ , see Fig. 4(b)] Stokes and anti-Stokes fields. The areas with negative values of the corresponding quasi-distributions  $P_{SA,s}^{\text{id}}$  are of the triangular form, as shown in Figs. 4(c,d). If the mean photon numbers of the Stokes and anti-Stokes modes are unbalanced, the negative triangular areas get a characteristic tilt [compare the graphs in Figs. 4(c) and 4(d)].

According to Eq. (33), the fields intensities at  $|\alpha_{L,m}^n|$ ,  $m = 1, \dots$ , are not bounded for the ratio  $\epsilon = 1$ , i.e., when the Stokes and anti-Stokes coupling constants equal. The fields intensities monotonically decrease with the increasing ratio  $\epsilon$  [see Fig. 5(a)]. The ratio  $\epsilon$  also influences the other fields parameters, as described by the following formulas:

$$\begin{aligned} g_{SA}^{(2)\text{id},m} &= (\epsilon^2 + 6\epsilon + 1)/(4\epsilon), \\ R_{SA}^{\text{id},m} &= 0, \\ \lambda_{SA}^{\text{id},m} &= (\sqrt{\epsilon} - 1)^2/(\sqrt{\epsilon} + 1)^2, \\ E_{N,SA}^{\text{id},m} &= \max[0, -\ln(\lambda_{SA}^{\text{id},m})], \\ \tau_{SA}^{\text{id},m} &= \max[0, (1 - \lambda_{SA}^{\text{id},m})/2], \\ \mathcal{S}_{S \rightarrow A}^{\text{id},m} &= \mathcal{S}_{A \rightarrow S}^{\text{id},m} = \max\{0, \ln[(\epsilon^2 + 6\epsilon + 1)/(\epsilon - 1)^2]\}, \\ \mathcal{B}_{SA}^{\text{id},m} &= \max_{q, \mathcal{J}} \left\{ \exp\left[-\frac{4\mathcal{J}}{\lambda_{SA}^{\text{id},m}}\right] - \exp\left[-\frac{4q^2 \mathcal{J}}{\lambda_{SA}^{\text{id},m}}\right] \right. \\ &\quad \left. + 2 \exp\left[-\frac{2\mathcal{J}[(q^2 + 1)(\epsilon^2 + 6\epsilon + 1) - 8q\sqrt{\epsilon}(\epsilon + 1)]}{(\epsilon - 1)^2}\right] \right\}. \end{aligned} \quad (37)$$

Whereas the Stokes and anti-Stokes photons are perfectly paired ( $R_{SA}^{\text{id},m} = 0$ ) for any fields intensity [see Fig. 5(b)], the quantum phase correlations are ideal for  $\epsilon = 1$  ( $\lambda_{SA}^{\text{id},m} = 0$ ) and they monotonically decrease with the increasing ratio  $\epsilon$ . The phase correlations become classical ( $\lambda_{SA}^{\text{id},m} = 1$ ) in the limit  $\epsilon \rightarrow \infty$ . The entanglement between the Stokes and anti-Stokes fields, quantified either by the logarithmic negativity  $E_{N,SA}^{\text{id},m}$  or the non-classicality depth  $\tau_{SA}^{\text{id},m}$ , behave similarly and they disappear in this limit. The Stokes–anti-Stokes fields are maximally entangled for  $\epsilon = 1$ , they gradually loose their entanglement with the increasing  $\epsilon$  and, finally, they are classical for  $\epsilon \rightarrow \infty$ . The intensity correlation function  $g_{SA}^{(2)\text{id},m}$ , that quantifies the violation of the Cauchy-Schwarz inequality, behaves as a function of  $\epsilon$  in the opposed way. It does not indicate the Cauchy-Schwarz inequality violation for  $\epsilon = 1$  ( $g_{SA}^{(2)\text{id},m} = 2$ ), but its value monotonically increases with the increasing  $\epsilon$  which indicates the non-classicality of the fields. On the other hand, the noise-reduction-factor  $R_{SA}^{\text{id},m}$  equals zero for any

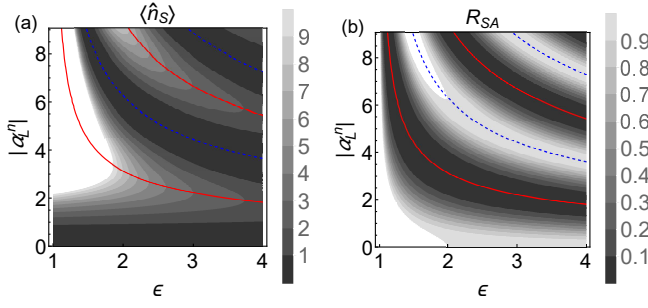


FIG. 5. (a) Stokes mean photon number  $\langle \hat{n}_S \rangle$  and (b) noise-reduction-factor  $R_{SA}$  as they depend on ratio  $\epsilon$  and normalized pump amplitude  $|\alpha_L^n|$ . The red solid [blue dashed] curves are given as  $|\alpha_{L,m}^n| = (2m-1)\pi/\sqrt{\epsilon-1}$  [ $|\tilde{\alpha}_{L,m}^n| = 2m\pi/\sqrt{\epsilon-1}$ ],  $m = 1, \dots$ , and identify local maxima (minima) in  $\langle \hat{n}_S \rangle$  and minima (maxima) in  $R_{SA}$ . The used parameters are:  $\epsilon = 4$ ,  $\gamma^n = 0$ ,  $n_V = n_T = 0$ .

$\epsilon$  owing to perfect pairing of the Stokes and anti-Stokes photons. The steering in the Stokes–anti-Stokes coupled system is symmetric, as we have  $\mathcal{S}_{S \rightarrow A}^{\text{id},m} = \mathcal{S}_{A \rightarrow B}^{\text{id},m}$ . According to Eq. (37), the greater the fields intensities are, the more pronounced the steering is. The behavior of intensity correlation function  $g_{SA}^{(2),\text{id},m}$  and noise-reduction-factor  $R_{SA}^{\text{id},m}$  in the limit  $\epsilon \rightarrow \infty$  in which they indicate the non-classicality, originates in the fact that the fields photon numbers  $\langle \hat{n}_S \rangle^{\text{id},m} = \langle \hat{n}_A \rangle^{\text{id},m}$  tend to zero in this limit and they occur in the denominators of fractions giving the discussed quantities. We note that such behavior is also observed in parametric down-conversion when it develops from the vacuum state. This means that these parameters are not suitable quantities for the characterization of the field properties for very low photon numbers.

## V. THE RAMAN PROCESS WITH AN IDEAL INITIALLY POPULATED VIBRATIONAL MODE

In the Raman process, there exist two mechanisms that influence the ideal process discussed in the previous section. The vibrational mode is in a thermal state with a nonzero mean phonon number and its dynamics suffers from the losses and the related additional noise.

The initial mean phonon number  $n_V$  increases with the temperature of the Raman medium and it is given by the Bose-Einstein formula. Such phonons then allow the emission of anti-Stokes photons without the preceding emission of a phonon in the Stokes interaction. Such anti-Stokes photons thus have no correlation to the Stokes photons and they weaken the entanglement between the Stokes and anti-Stokes fields. Using the solution in Eqs. (7), we can derive the following expressions for the coefficients of the normal characteristic function  $\mathcal{C}_{\mathcal{N}}$  and mean vibrational phonon number

$\langle \hat{n}_V \rangle(z) = B_V(z)$  in the oscillatory regime,

$$\begin{aligned} B_A^{\text{vib},p}(z) &= B_A^{\text{id},p}(z) + \epsilon n_V \beta(z), \\ B_S^{\text{vib},p}(z) &= B_S^{\text{id},p}(z) + n_V \beta(z), \\ D_{SA}^{\text{vib},p}(z) &= D_{SA}^{\text{id},p}(z) - 2\sqrt{\epsilon} n_V \beta(z), \\ B_V^{\text{vib},p}(z) &= n_V \cos^2(g_S z \sqrt{\epsilon-1}) + \beta(z), \\ \beta(z) &= \sin^2(g_S z \sqrt{\epsilon-1}) / (\epsilon-1), \end{aligned} \quad (38)$$

using the coefficients in Eqs. (31). According to Eqs. (38), the thermal vibrational phonons increase the mean number  $\langle \hat{n}_S \rangle$  of Stokes photons owing to the stimulated emission in the Stokes interaction accompanied by the generation of additional phonons [see Fig. 6(a)]. The thermal vibrational phonons are also responsible for the generation of additional anti-Stokes photons, but this is accompanied by the annihilation of phonons. Whereas the mean number  $\langle \hat{n}_A \rangle$  of anti-Stokes photons increases owing to the presence of vibrational thermal phonons, the mean number of vibrational phonons  $\langle \hat{n}_V \rangle(z)$  may increase or decrease as the Raman process proceeds. Detailed analysis of the formula in Eq. (38) reveals that for  $n_V < 1/(\epsilon-1)$  [ $n_V > 1/(\epsilon-1)$ ] the number of vibrational phonons  $\langle \hat{n}_V \rangle(z)$  first increases [decreases] and then it decreases [increases]. This behavior originates in the fact that the effective strength of the Stokes interaction quantified by the probability  $p_{SA}(1,0)$  is greater than that of the anti-Stokes interaction quantified by the probability  $p_{SA}(0,1)$  for  $n_V < 1/(\epsilon-1)$ . On the other hand, the anti-Stokes interaction is stronger than the Stokes one for  $n_V > 1/(\epsilon-1)$ , as documented in Figs. 4(e,f).

The greatest values of the Stokes mean photon number  $\langle \hat{n}_S \rangle$  as well as the logarithmic negativity  $E_{\mathcal{N},SA}$  are found for the pump amplitudes  $|\alpha_{L,m}^n| = (2m-1)\pi/\sqrt{\epsilon-1}$ ,  $m = 1, 2, \dots$ , in accordance with the ideal case. Also here, the mean number  $\langle \hat{n}_A \rangle$  of anti-Stokes photons equals that of the Stokes photons. A bit surprisingly, the greatest Stokes and anti-Stokes mean photon numbers  $\langle \hat{n}_S \rangle^m$  and  $\langle \hat{n}_A \rangle^m$ , respectively, are equal and coincide with those of the ideal case. The mean phonon number  $\langle \hat{n}_V \rangle^m$  for this case equals the initial one, as it follows from the conservation law of photon/phonon numbers in Eq. (6). This property originates in the general form of the system dynamics without phonon damping that predicts periodicity in the evolution of the vibrational mode two times faster than that of the Stokes and anti-Stokes modes [see Eqs. (31) and (38)]. This means that when the vibrational mode returns for the first time to its initial state, the Stokes and anti-Stokes modes are left in certain nontrivial state. The conservation of the photon/phonon numbers as expressed in Eq. (6) then gives the same mean photon numbers for both Stokes and anti-Stokes modes.

The thermal phonons drive the Stokes–anti-Stokes dynamics towards greater mixedness [see the purity  $\mu_{SA}$  in Fig. 6(f)] first, but the combined Stokes–anti-Stokes field returns back into a pure state later. This results in considerably nonclassical values of the  $g_{SA}^{(2),m}$  inten-

sity function [see Fig. 6(b)], noise-reduction-factor  $R_{SA}^m$  [Fig. 6(c)], two-mode principal squeezing variance  $\lambda_{SA}^m$  [Fig. 6(d)] and logarithmic negativity  $E_{N,SA}^m$  [Fig. 6(e)]. Nonzero mean phonon numbers  $n_V$  also cause the loss of the ability to steer both the Stokes and anti-Stokes modes for small pump amplitudes  $|\alpha_L^n|$  [see Figs. 6(g,h)]. This ability is restored for larger values of the pump amplitude  $|\alpha_L^n|$ . The steering by the Stokes mode appears for smaller values of the pump amplitude  $|\alpha_L^n|$  compared to that by the anti-Stokes mode. However, and the most importantly, for the pump amplitudes  $|\alpha_{L,m}^n|$ , for which the Stokes and anti-Stokes modes are equally populated, the combined Stokes–anti-Stokes state is pure and identical to that in Eq. (34) found in the ideal case ( $n_V = 0$ ). Also, for the pump amplitudes  $|\alpha_{L,m}^n|$  the Bell parameter  $\mathcal{B}_{SA}$  reaches its maximal value independently on the value of  $n_V$  [see Fig. 6(i)].

We note that, using the formulas (31) and (38), the ratio  $\mathcal{R} \equiv \langle \hat{n}_A \rangle / \langle \hat{n}_S \rangle$  of the anti-Stokes and Stokes mean photon numbers can be written as a Taylor expansion in the pump intensity  $|\alpha_L^n|^2$ :

$$\mathcal{R} = \frac{B_A}{B_S} \approx \frac{\epsilon n_V}{n_V + 1} + \frac{\epsilon}{4(n_V + 1)} \left( 1 - \frac{\epsilon n_V}{n_V + 1} \right) |\alpha_L^n|^2. \quad (39)$$

According to Eq. (39) the experimental determination of the ratio  $\mathcal{R}$  as it depends on the pump intensity  $|\alpha_L^n|^2$  gives us the ratio  $\epsilon$  of the anti-Stokes and Stokes coupling constants as well as the mean number  $n_V$  of thermal phonons. If the constants  $r_a$  and  $r_b$  in the experimental function  $\mathcal{R} = r_a + r_b |\alpha_L^n|^2$  are known, we have  $\epsilon = r_a + 4r_b/(1 - r_a)$  and  $n_V = r_a(1 - r_a)/(4r_b)$ .

The Stokes and anti-Stokes fields also exhibit spatially nonlocal correlations in their intensities. They are characterized by the correlation function  $\langle \Delta I_S(z_S) \Delta I_A(z_A) \rangle$  of the Stokes  $[\Delta I_S(z_S)]$  and anti-Stokes  $[\Delta I_A(z_A)]$  intensity fluctuations at positions  $z_S$  and  $z_A$ , respectively, that is derived in the form:

$$\langle \Delta I_S(z_S) \Delta I_A(z_A) \rangle = |d_{SA}(z_S, z_A)|^2. \quad (40)$$

The formula for the coefficient  $d_{SA}(z_S, z_A)$  in Eq. (11) considered for the zero-temperature reservoir ( $n_T = 0$ ) expresses this correlation as an interference of two factorized terms. Whereas only the second term is nonzero for  $n_V = 0$ , the first term dominates the second one for large  $n_V$ . In both limiting cases, the correlation function  $\langle \Delta I_S(z_S) \Delta I_A(z_A) \rangle$  is factorized as a function of the positions  $z_S$  and  $z_A$ . This leads to specific factorized forms of the correlation function  $\langle \Delta I_S(z_S) \Delta I_A(z_A) \rangle$ , as shown in Figs. 7(a,c). Factorization of the correlation function means that, from the point of view of this correlation function, the Stokes and anti-Stokes fields are independent. For nonzero mean vibrational phonon numbers  $n_V$ , the Stokes and anti-Stokes intensities are correlated and they form a typical tilted interference pattern, as documented in Fig. 7(b). Both types of the interference patterns are 2D periodic. However, if the vibrational mode is damped, the 2D periodicity is lost. In this case, ef-

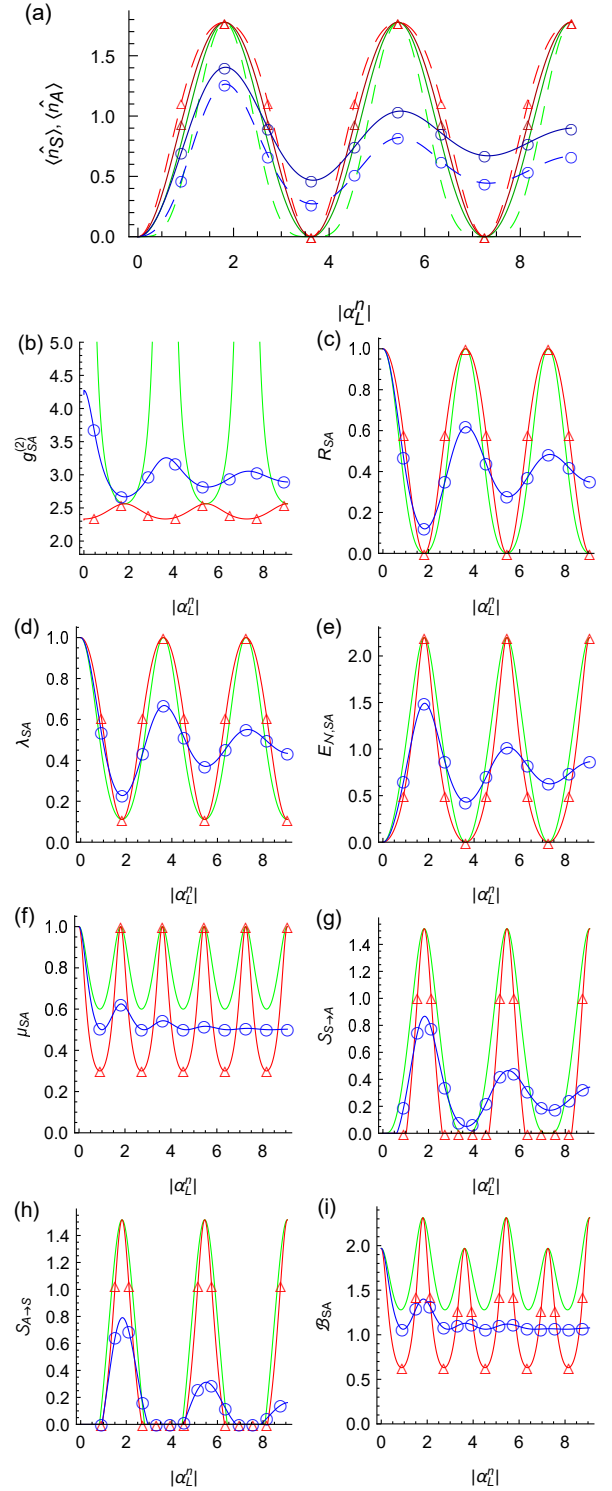


FIG. 6. (a) Stokes ( $\langle \hat{n}_S \rangle$ , dark solid curves) and anti-Stokes ( $\langle \hat{n}_A \rangle$ , light dashed curves) mean photon numbers, (b)  $g_{SA}^{(2)}$  intensity function, (c) noise-reduction-factor  $R_{SA}$ , (d) principal squeezing variance  $\lambda_{SA}$ , (e) logarithmic negativity  $E_{N,SA}$ , (f) purity  $\mu_{SA}$ , (g,h) steering parameters  $\mathcal{S}_{S \rightarrow A}$  (g) and  $\mathcal{S}_{A \rightarrow S}$  (h) and (i) the Bell parameter  $\mathcal{B}_{SA}$  as they depend on normalized pump amplitude  $|\alpha_L^n|$ . The used parameters are:  $\epsilon = 4$ ;  $n_V = n_T = 0$ ,  $\gamma^n = 0$  (green plain curves);  $n_V = 0.5$ ,  $\gamma^n = 0$ ,  $n_T = 0$  (red curves with  $\Delta$ );  $n_V = n_T = 0.1$ ,  $\gamma/(\bar{g}_S |\alpha_L|) = 1$  (blue curves with  $\circ$ ).

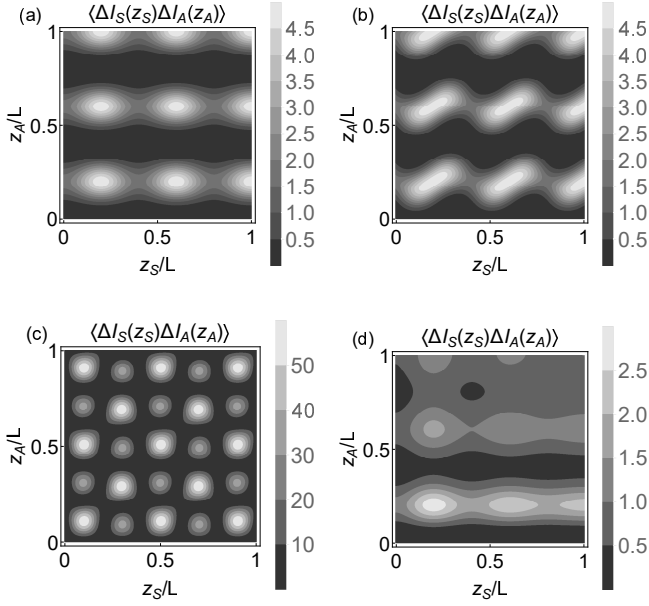


FIG. 7. Correlation function  $\langle \Delta I_S(z_S) \Delta I_A(z_A) \rangle$  as it depends on positions  $z_S$  and  $z_A$  in the Stokes and anti-Stokes fields for (a)  $n_V = 0$ ,  $\gamma^n = 0$ , (b)  $n_V = 1$ ,  $\gamma^n = 0$ , (c)  $n_V = 10$ ,  $\gamma^n = 0$ , (d)  $n_V = 0$ ,  $\gamma/(\tilde{g}_S|\alpha_L|) = 1$ ;  $\epsilon = 4$ ,  $n_T = 0$  and  $\tilde{g}_S|\alpha_L| = 5\pi/\sqrt{\epsilon-1}$ .

fective damping in the anti-Stokes mode is stronger than that in the Stokes mode, as evidenced in Fig. 7(d).

## VI. THE RAMAN PROCESS WITH A POPULATED AND DAMPED VIBRATIONAL MODE

Contrary to the influence of the thermal mean phonon number  $n_V$ , damping of the vibrational mode and the accompanying noise (the fluctuation-dissipation theorem) cause irreversible changes in the dynamics of the Stokes and anti-Stokes fields. The above discussed periodic dependence of the analyzed quantities on the pump amplitude  $|\alpha_L^n|$  is replaced by that with fixed asymptotic values in the limiting case  $|\alpha_L^n| \rightarrow \infty$  [see Fig. 6]. Damping in the vibrational mode decreases the maximal attainable mean photon numbers  $\langle \hat{n}_A \rangle$  and  $\langle \hat{n}_S \rangle$  [see Fig. 6(a)] and weakens quantum correlations between the Stokes and anti-Stokes fields [see the logarithmic negativity  $E_{\mathcal{N},SA}$  in Fig. 6(e)]. Damped oscillations still occur in the mean photon numbers  $\langle \hat{n}_A \rangle$  and  $\langle \hat{n}_S \rangle$  and logarithmic negativity  $E_{\mathcal{N},SA}$  considered as a function of the pump amplitude  $|\alpha_L^n|$ . Their period is larger compared to the ideal case and it increases with the increasing damping constant  $\gamma$ , as it follows from the analytical formulas in Eqs. (7) that give the corresponding frequency  $\omega = \sqrt{|g_A|^2 - |g_S|^2 - \gamma^2}$ . With the increasing pump amplitude  $|\alpha_L^n|$ , the common state of the Stokes and anti-Stokes modes loses its purity  $\mu_{SA}$  and reaches its asymptotic value fast [see Fig. 6(f)]. Damping of the vi-

brational mode also reduces the non-classicality of the combined Stokes-anti-Stokes field observed via the  $g_{SA}^{(2)}$  intensity function [see Fig. 6(b)], noise-reduction-factor  $R_{SA}$  [Fig. 6(c)] and two-mode principal squeezing variance  $\lambda_{SA}$  [Fig. 6(d)]. Moreover, it causes large unbalance in the steering property between the Stokes and anti-Stokes modes, as documented in Figs. 6(g,h). Especially, the ability of the anti-Stokes mode to steer the Stokes mode is considerably reduced. Further, the Bell violation is only observed for small values of  $\gamma^n$ ; it is not observed for the value of  $\gamma^n$  used in Fig. 6(i).

In the asymptotic limit  $|\alpha_L^n| \rightarrow \infty$ , the coefficients in the normal characteristic function  $C_{\mathcal{N}}$  attain the form:

$$\begin{aligned} B_A^{\text{asym}} &= (\epsilon n'_T + \epsilon) / (\epsilon - 1)^2, \\ B_S^{\text{asym}} &= (n'_T + 2\epsilon - 1) / (\epsilon - 1)^2, \\ D_{SA}^{\text{asym}} &= -\sqrt{\epsilon} (n'_T + \epsilon) / (\epsilon - 1)^2. \end{aligned} \quad (41)$$

and  $n'_T \equiv (\epsilon - 1)n_T$ .

Then, the purity  $\mu_{SA}^{\text{asym}}$  is derived in the form:

$$\mu_{SA}^{\text{asym}} = \frac{(\epsilon - 1)^2}{(\epsilon + 1)(\epsilon - 1 + 2n'_T)}. \quad (42)$$

If  $\epsilon = 1$ , i.e., the Stokes and anti-Stokes interactions are balanced, the asymptotic state is maximally mixed. The increasing ratio  $\epsilon$ , that effectively partially decouples the anti-Stokes mode, improves the purity of the asymptotic state. On the other hand, the greater the mean reservoir phonon number  $n_T$  is the worse the purity of the asymptotic state is.

The entanglement of the asymptotic Stokes and anti-Stokes fields quantified either by the logarithmic negativity  $E_{\mathcal{N},SA}^{\text{asym}}$  or the non-classicality depth  $\tau_{SA}^{\text{asym}}$ ,

$$\begin{aligned} E_{\mathcal{N},SA}^{\text{asym}} &= \max\{0, \ln[(s_1 - 4s_2\sqrt{s_3})/2] / 2\}, \\ \tau_{SA}^{\text{asym}} &= \max\{0, (1 - s_2 + \sqrt{s_3})/2\}, \\ s_1 &= 2(\epsilon + 1)[(\epsilon^3 + 5\epsilon^2 - 3\epsilon + 1) + 2(\epsilon^2 + 4\epsilon - 1)n'_T \\ &\quad + 2(\epsilon + 1)n_T'^2] / (\epsilon - 1)^4, \\ s_2 &= 4(\epsilon + 1)(\epsilon + n'_T) / (\epsilon - 1)^2, \\ s_3 &= [(4\epsilon^3 + \epsilon^2 - 2\epsilon + 1) + 2(\epsilon + 1)(3\epsilon - 1)n'_T \\ &\quad + (\epsilon + 1)^2 n_T'^2] / (\epsilon - 1)^4, \end{aligned} \quad (43)$$

weakens with the increasing ratio  $\epsilon$  as well as the increasing mean reservoir phonon number  $n_T$ . Detailed analysis of the formulas (43) reveals that all asymptotic states are entangled for  $\epsilon > 1$  and  $n_T \geq 0$ .

The quantum correlations of the asymptotic states can directly be monitored via the  $g_{SA}^{(2),\text{asym}}$  intensity function, noise-reduction-factor  $R_{SA}^{\text{asym}}$  and principal squeezing variance  $\lambda_{SA}^{\text{asym}}$ :

$$\begin{aligned} g_{SA}^{(2),\text{asym}} &= \frac{\epsilon^2 + 2\epsilon - 1 + 4\epsilon n'_T + 2n_T'^2}{(n'_T + 1)(n'_T + 2\epsilon - 1)}, \\ R_{SA}^{\text{asym}} &= \frac{\epsilon + (\epsilon - 1)n'_T + n_T'^2}{3\epsilon - 1 + (\epsilon + 1)n'_T}, \\ \lambda_{SA}^{\text{asym}} &= [\epsilon + n'_T] / (\sqrt{\epsilon} + 1)^2. \end{aligned} \quad (44)$$



Whereas the  $g_{SA}^{(2),\text{asym}}$  function indicates the non-classicality for  $\epsilon > 1$  ( $g_{SA}^{(2),\text{asym}} > 2$ ), nonclassical values of the noise-reduction-factor  $R_{SA}^{\text{asym}}$  occur only for  $n_T \in \langle 0, (\sqrt{2\epsilon} + 1)/(\epsilon - 1) \rangle$  ( $R_{SA}^{\text{asym}} < 1$ ) and, similarly, nonclassical values of the principal squeezing variance  $\lambda_{SA}^{\text{asym}}$  are observed only when  $n_T \in \langle 0, (2\sqrt{\epsilon} + 1)/(\epsilon - 1) \rangle$  ( $\lambda_{SA}^{\text{asym}} < 1$ ). It holds for all three quantities, that the greater the mean reservoir phonon number  $n_T$  is, the less nonclassical their values are. Also, the greater the ratio  $\epsilon$  is the less nonclassical the values of  $\lambda_{SA}^{\text{asym}}$  are.

Provided that  $n_T \in \langle 0, 1/(\epsilon - 1) \rangle$  steering occurs in the asymptotic state as the analysis of the underlying formulas reveals:

$$\begin{aligned} \mathcal{S}_{S \rightarrow A}^{\text{asym}} &= \max \left\{ 0, \ln \left[ \frac{\epsilon^2 + 2\epsilon - 1 + 2n'_T}{(\epsilon + 1)(\epsilon - 1 + 2n'_T)} \right] \right\}, \\ \mathcal{S}_{A \rightarrow S}^{\text{asym}} &= \max \left\{ 0, \ln \left[ \frac{\epsilon^2 + 1 + 2\epsilon n'_T}{(\epsilon + 1)(\epsilon - 1 + 2n'_T)} \right] \right\}. \end{aligned} \quad (45)$$

The Stokes mode steers the anti-Stokes mode and vice versa in this case though the steering of the anti-Stokes mode is stronger than the steering of the Stokes mode. The increasing mean reservoir phonon number  $n_T$  weakens the ability to steer. The Bell nonlocality was not observed in the discussed steady state.

The ratio  $\mathcal{R}^{\text{asym}} \equiv \langle \hat{n}_A \rangle^{\text{asym}} / \langle \hat{n}_S \rangle^{\text{asym}}$  of the anti-Stokes and Stokes mean photon numbers derived for the asymptotic state as

$$\mathcal{R}^{\text{asym}} = \frac{B_A^{\text{asym}}}{B_S^{\text{asym}}} = \frac{\epsilon + \epsilon(\epsilon - 1)n_T}{2\epsilon - 1 + (\epsilon - 1)n_T} \quad (46)$$

can conveniently be used to experimentally determine the ratio  $\epsilon$ . If the mean number  $n_T$  of reservoir phonons can be neglected, we have

$$\epsilon = \mathcal{R}^{\text{asym}} / (2\mathcal{R}^{\text{asym}} - 1). \quad (47)$$

Provided that  $n_T > 0$  we obtain a quadratic equation for  $\epsilon$ .

We note that, in the real Raman process, the Stokes and anti-Stokes fields may suffer from additional scattering, e.g., on the Raman crystal edges and imperfections. This scattering which means an additional dissipation in the system can be taken into account similarly as we have done for the vibrational mode [17]. This leads to weakening of the entanglement and other non-classical properties of the Stokes and anti-Stokes fields.

At the end, we mention generalization of the developed model towards real experimental conditions. The developed model is stationary. It has been formulated for monochromatic plane waves whose harmonic dependence along the  $z$  axis is modified by the nonlinear Stokes and anti-Stokes interactions. A more realistic model should involve non-stationary fields, both in time and the transverse plane of the interacting fields. This can be done by considering spectrally and spatially multi-mode fields. In the simplest approximation, we may model such fields

by independent quadruples of spatio-spectral modes in the laser, Stokes, anti-Stokes, and vibrational modes, similarly as it was done in [47] for parametric down-conversion. The results obtained for the developed model can then be applied for each quadruple of modes that differ by their material parameters  $(\epsilon, |\alpha_{L,m}^n|)$ . As the optimal normalized pump amplitudes  $|\alpha_{L,m}^n|$  of quadruples differ, not all the modes constituting the Stokes and anti-Stokes fields can simultaneously be under the conditions of ideal photon pairing. This results in weakening the nonclassical properties of the Stokes and anti-Stokes fields. The loss of non-classicality depends on detailed conditions of the Raman process. Here, to illustrate the loss of non-classicality we consider the behavior of the noise-reduction-factor  $R_{SA}^m$  defined in Eq. (17) and written for multi-mode fields as

$$R_{SA}^m = \frac{\langle (\Delta[\hat{N}_S - \hat{N}_A])^2 \rangle}{\langle \hat{N}_S \rangle + \langle \hat{N}_A \rangle} \quad (48)$$

where  $\hat{N}_b = \sum_{j=1}^{M_b} \hat{n}_{b,j}$  gives the overall photon-number operator in field  $b$  composed of  $M_b$  modes,  $b = S, A$ . In Fig. 8(a), we quantify the loss of ideal pairing of the Stokes and anti-Stokes photons with the increasing number of modes described by parameter  $\delta$  that defines constant nonzero density of modes in the neighborhood of the optimal normalized pump amplitude  $|\alpha_{L,1}^n|$  defined as  $|\alpha_L^n| \in |\alpha_{L,1}^n| \langle 1 - \delta/2, 1 + \delta/2 \rangle$ . The curve in Fig. 8(a) for the Raman process with the ideal vibrational mode in the initial vacuum state was drawn along the following formula derived from Eqs. (31):

$$R_{SA}^m = \frac{2\pi\delta(4\epsilon - 1) - 8\epsilon \sin(\pi\delta) + \sin(2\pi\delta)}{8 \left[ \pi\delta(7\epsilon - 1) + 16\epsilon \sin\left(\frac{\pi\delta}{2}\right) + (\epsilon + 1) \sin(\pi\delta) \right]}. \quad (49)$$

According to the curves in Fig. 8(a), the greater the number of modes linearly proportional to the parameter  $\delta$  is, the greater the loss of non-classicality is. Also, the presence of thermal vibrational phonons results in the faster loss of non-classicality with the increasing number of modes: Assuming the value of parameter  $\epsilon$  fixed, the greater the number  $n_V$  of initial thermal phonons is, the greater the value of the noise-reduction-factor  $R_{SA}^m$  is [see Fig. 8(b)].

## VII. CONCLUSIONS

The ability of the Raman process to form nonclassical correlations between the Stokes and anti-Stokes fields has been analyzed. The quantum model involving independent Stokes and anti-Stokes interactions has been developed using the operator solution of the Heisenberg equations. According to the model, if damping of the vibrational mode in the thermal state is negligible and the anti-Stokes nonlinear interaction is stronger than the Stokes one, the Stokes and anti-Stokes fields are composed of only photon pairs for specific laser pump amplitudes. In the intensity properties, the generated state

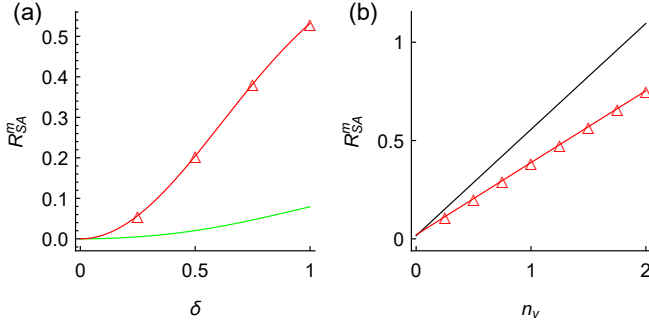


FIG. 8. Noise-reduction-factor  $R_{SA}^m$  as it depends on (a) the number of modes described by parameter  $\delta$  and (b) initial mean phonon number  $n_V$ . Constant density of modes is assumed for  $|\alpha_L^n| \in |\alpha_{L,1}^n|(1 - \delta/2, 1 + \delta/2)$ ; (a)  $\epsilon = 4$ ,  $\gamma^n = 0$ ,  $n_V = n_T = 0$  (green plain curve),  $n_V = 0.5$  (red curve with  $\triangle$ ) and (b)  $\gamma^n = 0$ ,  $n_T = 0$ ,  $\delta = 1/2$ ,  $\epsilon = 2$  (black plain curve),  $\epsilon = 4$  (red curve with  $\triangle$ ).

is equivalent to the state of an ideal twin beam with the same intensity. The state is thus highly entangled, exhibits strong sub-shot-noise correlations in the difference of the Stokes and anti-Stokes photon numbers, two-mode phase squeezing, steering and the Bell nonlocal correlations. The needed pump amplitudes depend on the length of the medium and nonlinear coupling constants. The mean Stokes and anti-Stokes photon numbers in this state are independent of the mean number of thermal vibrational phonons, but they vary with the ratio of the anti-Stokes and Stokes coupling constants.

When damping of the vibrational mode is considered as well as the pump amplitude differs from the above ideal ones, the states of the combined Stokes and anti-Stokes fields become mixed, but they still exhibit nonclassical features though these are weaker compared to those of the ideal twin beams. Asymmetry between the Stokes and anti-Stokes fields belongs to the most important features of these states: The Stokes field has stronger influence to the anti-Stokes field than the anti-Stokes field influences the Stokes field.

The obtained results elucidate the important role of the anti-Stokes field and its correlations with the Stokes field in the Raman process. This may find application in more detailed characterization of the vibrational mode, which is the essence of the Raman spectroscopy. Moreover, under suitable conditions the Raman process generates ideally paired optical fields that are commonly used in quantum metrology and various quantum-information protocols. Compared to parametric down-conversion usually used in photon-pair generation, the Raman process is more complex, but also more versatile. This may be useful, e.g., in quantum metrology.

## ACKNOWLEDGEMENTS

The authors thank J. Peřina for fruitful discussions and reading the manuscript. They acknowledge GA ĆR (project No. 18-22102S) and support from ERDF/ESF project ‘Nanotechnologies for Future’ (CZ.02.1.01/0.0/0.0/16\_019/0000754).

## Appendix A: Spontaneous parametric down-conversion

The process of spontaneous parametric down-conversion pumped by a strong classical laser beam with amplitude  $|\alpha_L| \exp(i\varphi_L) \exp(ik_L z - i\omega_L t)$  is described by the following momentum operator  $\hat{G}_{\text{spdc}}(z)$  [70]:

$$\begin{aligned} \hat{G}_{\text{spdc}}(z) = & \hbar k_s \hat{a}_s^\dagger(z) \hat{a}_s(z) + \hbar k_i \hat{a}_i^\dagger(z) \hat{a}_i(z) \\ & + \left[ (\hbar \tilde{g} \hat{a}_s^\dagger(z) \hat{a}_i^\dagger(z) |\alpha_L| \exp(ik_L z + i\phi_L) + \text{H.c.} \right]. \end{aligned} \quad (\text{A1})$$

The annihilation (creation) operators  $\hat{a}_s$  and  $\hat{a}_i$  ( $\hat{a}_s^\dagger$  and  $\hat{a}_i^\dagger$ ) are defined in the signal and idler modes, respectively. Symbol  $\tilde{g}$  denotes the nonlinear coupling constant. The frequencies  $\omega_s$  and  $\omega_i$  of the signal and idler modes, respectively, obey the relation  $\omega_s + \omega_i = \omega_L$ . We also assume the phase-matching conditions for the signal and idler wave vectors  $k_s$  and  $k_i$ , i.e.  $k_s + k_i = k_L$ .

The Heisenberg equations derived from the momentum operator  $\hat{G}_{\text{spdc}}(z)$  take the form:

$$\begin{aligned} \frac{d\hat{a}_s(z)}{dz} &= ik_s \hat{a}_s(z) + g \hat{a}_i^\dagger(z) \exp(ik_L z), \\ \frac{d\hat{a}_i(z)}{dz} &= ik_i \hat{a}_i(z) + g \hat{a}_s^\dagger(z) \exp(ik_L z) \end{aligned} \quad (\text{A2})$$

and  $g = i\tilde{g}|\alpha_L| \exp(i\phi_L)$ . Introducing the operators  $\hat{A}_b(z) \equiv \hat{a}_b(z) \exp(-ik_b z)$ ,  $b = s, i$ , and assuming  $\phi_L = -\pi/2$  to make the nonlinear coupling constant  $g$  real and positive, the solution to Eqs. (A2) is expressed as [70]:

$$\begin{aligned} \hat{A}_s(z) &= \tilde{f}_1(z) \hat{A}_s(0) + \tilde{f}_2(z) \hat{A}_i^\dagger(0), \\ \hat{A}_i(z) &= \tilde{f}_1(z) \hat{A}_i(0) + \tilde{f}_2(z) \hat{A}_s^\dagger(0), \end{aligned} \quad (\text{A3})$$

where

$$\tilde{f}_1(z) = \cosh(gz), \quad \tilde{f}_2(z) = \sinh(gz). \quad (\text{A4})$$

The coefficients in the normal characteristic function  $C_N$  in Eq. (9) attain for this solution and the initial vacuum states the form:

$$\begin{aligned} B_s(z) &= B_i(z) = \tilde{f}_2^2(z), \\ D_{si}(z) &= \tilde{f}_1(z) \tilde{f}_2(z). \end{aligned} \quad (\text{A5})$$

## Appendix B: Statistical operator of the Stokes–anti-Stokes field in the ‘balanced’ condition

Here we consider the vibrational mode without damping and being in the initial vacuum state. Under these conditions, in the oscillatory regime with the pump amplitudes  $|\alpha_{L,m}^n| = (2m-1)\pi/\sqrt{\epsilon-1}$ ,  $m = 1, 2, \dots$ , the mean numbers of Stokes and anti-Stokes photons coincide and we have:

$$\begin{aligned} B^{\text{id},m} &= \langle \hat{n}_S \rangle^{\text{id},m} = \langle \hat{n}_A \rangle^{\text{id},m} = 4\epsilon/(\epsilon-1)^2, \\ D_{SA}^{\text{id},m} &= -2\sqrt{\epsilon}(\epsilon+1)/(\epsilon-1)^2; \end{aligned} \quad (\text{B1})$$

$|D_{SA}^{\text{id},m}|^2 = B^{\text{id},m}(B^{\text{id},m}+1)$ . The anti-normal characteristic function  $C_A$  [14] is then derived in the form:

$$\begin{aligned} C_A(\beta_S, \beta_A) &\equiv \exp[-|\beta_S|^2 - |\beta_A|^2] C_N(\beta_S, \beta_A) \\ &= \exp[-(B^{\text{id},m}+1)(|\beta_S|^2 + |\beta_A|^2)] \\ &\quad \times \exp[D_{SA}^{\text{id},m} \beta_S^* \beta_A^* + \text{c.c.}]. \end{aligned} \quad (\text{B2})$$

Its Fourier transform, the anti-normal distribution function  $P_A$  defined as

$$\begin{aligned} P_A(\alpha_S, \alpha_A) &= \frac{1}{\pi^2} \int d^2\beta_S d^2\beta_A C_A(\beta_S, \beta_A) \\ &\quad \times \exp[\alpha_S \beta_S^* + \alpha_A \beta_A^* - \text{c.c.}] \end{aligned} \quad (\text{B3})$$

takes the form [14]:

$$P_A(\alpha_S, \alpha_A) = \frac{1}{\pi^2(B^{\text{id},m}+1)} \exp[-|\alpha_S|^2 - |\alpha_A|^2]$$

$$\times \exp[\tilde{D}_{SA}^{\text{id},m*} \alpha_S \alpha_A] \exp[\tilde{D}_{SA}^{\text{id},m} \alpha_S^* \alpha_A^*]; \quad (\text{B4})$$

$$\tilde{D}_{SA}^{\text{id},m} = \sqrt{B^{\text{id},m}/(B^{\text{id},m}+1)}.$$

On the other hand, the relation [14]

$$P_A(\alpha_S, \alpha_A) = \frac{1}{\pi^2} \langle \alpha_S \alpha_A | \hat{\varrho} | \alpha_S \alpha_A \rangle \quad (\text{B5})$$

allows us to express the anti-normal distribution function  $P_A$  in terms of the elements  $\langle m_S m_A | \hat{\varrho} | n_S n_A \rangle$  of the statistical operator  $\hat{\varrho}$  in the Fock basis:

$$\begin{aligned} P_A(\alpha_S, \alpha_A) &= \frac{1}{\pi^2} \exp[-|\alpha_S|^2 - |\alpha_A|^2] \sum_{m_S, n_S=0}^{\infty} \sum_{m_A, n_A=0}^{\infty} \\ &\quad \langle m_S m_A | \hat{\varrho} | n_S n_A \rangle \frac{\alpha_S^{*m_S} \alpha_S^{n_S}}{\sqrt{m_S! n_S!}} \frac{\alpha_A^{*m_A} \alpha_A^{n_A}}{\sqrt{m_A! n_A!}}. \end{aligned} \quad (\text{B6})$$

Expanding the exponentials on the second line of Eq. (B4) into their Taylor series and comparing the expressions in Eqs. (B4) and (B6), we arrive at the formula for the elements of the statistical operator  $\hat{\varrho}$ :

$$\begin{aligned} \langle m_S m_A | \hat{\varrho} | n_S n_A \rangle &= \delta_{m_S m_A} \delta_{n_S n_A} \frac{[\tilde{D}_{SA}^{\text{id},m}]^{*m_S} [\tilde{D}_{SA}^{\text{id},m}]^{n_S}}{B^{\text{id},m}+1} \\ &= \delta_{m_S m_A} \delta_{n_S n_A} (-1)^{m_S+n_S} \frac{[B^{\text{id},m}]^{(m_S+n_S)/2}}{[B^{\text{id},m}+1]^{(m_S+n_S)/2+1}}. \end{aligned} \quad (\text{B7})$$

The statistical operator  $\hat{\varrho}$  thus describes a pure state written in Eq. (34) together with the corresponding photon-number distribution  $p_{SA}^{\text{id}}(n_S, n_A)$ .

- 
- [1] J. P. Dowling and G. J. Milburn, “Quantum technology: the second quantum revolution,” *Phil. Trans. R. Soc. A* **361**, 1655–1674 (2003).
  - [2] R. J. Glauber, “Coherent and incoherent states of the radiation field,” *Phys. Rev.* **131**, 2766 (1963).
  - [3] E. C. G. Sudarshan, “Equivalence of semiclassical and quantum mechanical descriptions of statistical light beams,” *Phys. Rev. Lett.* **10**, 277 (1963).
  - [4] C. H. Bennett, G. Brassard, C. Crépeau, R. Jozsa, A. Peres, and W. K. Wootters, “Teleporting an unknown quantum state via dual classical and Einstein-Podolsky-Rosen channels,” *Phys. Rev. Lett.* **70**, 1895 (1993).
  - [5] C. H. Bennett and S. J. Wiesner, “Communication via one- and two-particle operators on Einstein-Podolsky-Rosen states,” *Phys. Rev. Lett.* **69**, 2881 (1992).
  - [6] V. Giovannetti, S. Lloyd, and L. Maccone, “Advances in quantum metrology,” *Nature Photonics* **5**, 222 (2011).
  - [7] A. K. Ekert, “Quantum cryptography based on Bell’s theorem,” *Phys. Rev. Lett.* **67**, 661 (1991).
  - [8] C. Branciard, E. G. Cavalcanti, S. P. Walborn, V. Scarani, and H. M. Wiseman, “One-sided device-independent quantum key distribution: security, feasibility, and the connection with steering,” *Phys. Rev. A* **85**, 010301 (2012).
  - [9] A. Acin, N. Gisin, and L. Masanes, “From Bell’s theorem to secure quantum key distribution,” *Phys. Rev. Lett.* **97**, 120405 (2006).
  - [10] J. Peřina Jr., “Coherent light in intense spatio-spectral twin beams,” *Phys. Rev. A* **93**, 063857 (2016).
  - [11] L. Mandel and E. Wolf, *Optical Coherence and Quantum Optics* (Cambridge Univ. Press, Cambridge, 1995).
  - [12] C. V. Raman and K. S. Krishnan, “A new type of secondary radiation,” *Nature* **121**, 501–502 (1928).
  - [13] R. W. Boyd, *Nonlinear Optics, 2nd edition* (Academic Press, New York, 2003).
  - [14] J. Peřina and J. Křepelka, “Quantum statistics of stimulated Raman and hyper-Raman scattering of squeezed light with pump depletion,” *J. Mod. Opt.* **39**, 1029–1041 (1992).
  - [15] J. Peřina Jr. and J. Peřina, “Statistics of light in Raman and Brillouin nonlinear couplers,” *Quantum Semiclass. Opt.* **9**, 443–464 (1997).
  - [16] D. F. Walls, “Quantum theory of the Raman effect,” *Zeitschrift für Physik A Hadrons and Nuclei* **237**, 224–233 (1970).
  - [17] J. Peřina, *Quantum Statistics of Linear and Nonlinear Optical Phenomena* (Kluwer Academic, Dordrecht-Boston, 1991).
  - [18] A. Miranowicz and S. Kielich, “Quantum-statistical theory of Raman scattering processes,” in *Modern Nonlinear Optics*, Vol. 3 (John Wiley & Sons, New York, 1994) pp. 531–626.
  - [19] K. Thapliyal and J. Peřina, “Nonclassicality in off-resonant Raman process,” *Phys. Lett. A* **383**, 2011–2020 (2019).

- (2019).
- [20] K. Thapliyal, A. Pathak, B. Sen, and J. Peřina, “Lower- and higher-order nonclassical features in non-degenerate hyper-Raman processes,” *Opt. Commun.* **444**, 111–119 (2019).
  - [21] K. Thapliyal and J. Peřina, “Quasidistribution of phases in Raman process with weak and strong pumps,” *Phys. Scr.* **95**, 034001 (2020).
  - [22] M. Kasperczyk, F. S. de Aguiar Júnior, C. Rabelo, A. Saraiva, M. F. Santos, L. Novotny, and A. Jorio, “Temporal quantum correlations in inelastic light scattering from water,” *Phys. Rev. Lett.* **117**, 243603 (2016).
  - [23] L. Podhora, P. Obřil, I. Straka, M. Jeřek, and L. Slodička, “Nonclassical photon pairs from warm atomic vapor using a single driving laser,” *Opt. Express* **25**, 31230–31238 (2017).
  - [24] M. D. Anderson, S. T. Velez, K. Seibold, H. Flayac, V. Savona, N. Sangouard, and C. Galland, “Two-color pump-probe measurement of photonic quantum correlations mediated by a single phonon,” *Phys. Rev. Lett.* **120**, 233601 (2018).
  - [25] S. T. Velez, V. Sudhir, N. Sangouard, and C. Galland, “Bell correlations between light and vibration at ambient conditions,” *Sci. Adv.* **6**, eabb0260 (2020).
  - [26] F. S. de Aguiar Júnior, M. F. Santos, C. H. Monken, and A. Jorio, “Lifetime and polarization for real and virtual correlated Stokes-anti-Stokes Raman scattering in diamond,” *Phys. Rev. Research* **2**, 013084 (2020).
  - [27] A. Saraiva, F. S. de Aguiar Júnior, R. d. M. e Souza, A. P. Pena, C. H. Monken, M. F. Santos, B. Koiller, and A. Jorio, “Photonic counterparts of Cooper pairs,” *Phys. Rev. Lett.* **119**, 193603 (2017).
  - [28] F. S. de Aguiar Júnior, A. Saraiva, M. F. Santos, B. Koiller, R. d. M. e Souza, A. P. Pena, R. A. Silva, C. H. Monken, and A. Jorio, “Stokes-anti-Stokes correlated photon properties akin to photonic Cooper pairs,” *Phys. Rev. B* **99**, 100503 (2019).
  - [29] J.-P. Dou, A. I. Yang, M.-Y. Du, D. Lao, J. Gao, L.-F. Qiao, H. Li, X.-L. Pang, Z. Feng, H. Tang, *et al.*, “A broadband DLCZ quantum memory in room-temperature atoms,” *Commun. Phys.* **1**, 55 (2018).
  - [30] D.-S. Ding, “Raman quantum memory of photonic polarized entanglement,” in *Broad Bandwidth and High Dimensional Quantum Memory Based on Atomic Ensembles* (Springer, 2018) pp. 91–107.
  - [31] B. Jing, X.-J. Wang, Y. Yu, P.-F. Sun, Y. Jiang, S.-J. Yang, W.-H. Jiang, X.-Y. Luo, J. Zhang, X. Jiang, *et al.*, “Entanglement of three quantum memories via interference of three single photons,” *Nature Photonics* **13**, 210–213 (2019).
  - [32] L.-M. Duan, M. D. Lukin, J. I. Cirac, and P. Zoller, “Long-distance quantum communication with atomic ensembles and linear optics,” *Nature* **414**, 413–418 (2001).
  - [33] D. N. Matsukevich and A. Kuzmich, “Quantum state transfer between matter and light,” *Science* **306**, 663–666 (2004).
  - [34] P. Campagne-Ibarcq, E. Zalusky-Geller, A. Narla, S. Shankar, P. Reinhold, L. Burkhardt, C. Axline, W. Pfaff, L. Frunzio, R. J. Schoelkopf, *et al.*, “Deterministic remote entanglement of superconducting circuits through microwave two-photon transitions,” *Phys. Rev. Lett.* **120**, 200501 (2018).
  - [35] S. Chen, Y.-A. Chen, T. Strassel, Z.-S. Yuan, B. Zhao, J. Schmiedmayer, and J.-W. Pan, “Deterministic and storable single-photon source based on a quantum memory,” *Phys. Rev. Lett.* **97**, 173004 (2006).
  - [36] R. Riedinger, S. Hong, R. A. Norte, J. A. Slater, J. Shang, A. G. Krause, V. Anant, M. Aspelmeyer, and S. Gröblacher, “Non-classical correlations between single photons and phonons from a mechanical oscillator,” *Nature* **530**, 313 (2016).
  - [37] D. M. Meekhof, C. Monroe, B. E. King, W. M. Itano, and D. J. Wineland, “Generation of nonclassical motional states of a trapped atom,” *Phys. Rev. Lett.* **76**, 1796 (1996).
  - [38] A. Kuzmich, W. P. Bowen, A. D. Boozer, A. Boca, C. W. Chou, L.-M. Duan, and H. J. Kimble, “Generation of nonclassical photon pairs for scalable quantum communication with atomic ensembles,” *Nature* **423**, 731 (2003).
  - [39] K. C. Lee, B. J. Sussman, M. R. Sprague, P. Michelberger, K. F. Reim, J. Nunn, N. K. Langford, P. J. Bustard, D. Jaksch, and I. A. Walmsley, “Macroscopic non-classical states and terahertz quantum processing in room-temperature diamond,” *Nature Photonics* **6**, 41 (2012).
  - [40] S. T. Velez, K. Seibold, N. Kipfer, M. D. Anderson, V. Sudhir, and C. Galland, “Preparation and decay of a single quantum of vibration at ambient conditions,” *Phys. Rev. X* **9**, 041007 (2019).
  - [41] T. A. Eriksson, T. Hirano, B. J. Puttnam, G. Rademacher, R. S. Luís, M. Fujiwara, R. Namiki, Y. Awaji, M. Takeoka, N. Wada, *et al.*, “Wavelength division multiplexing of continuous variable quantum key distribution and 18.3 tbit/s data channels,” *Commun. Phys.* **2**, 1–8 (2019).
  - [42] X. Li, P. L. Voss, J. E. Sharping, and P. Kumar, “Optical-fiber source of polarization-entangled photons in the 1550 nm telecom band,” *Phys. Rev. Lett.* **94**, 053601 (2005).
  - [43] J. Fulconis, O. Alibart, W. Wadsworth, P. Russell, and J. Rarity, “High brightness single mode source of correlated photon pairs using a photonic crystal fiber,” *Opt. Express* **13**, 7572–7582 (2005).
  - [44] J. Fan, A. Migdall, and L. J. Wang, “Efficient generation of correlated photon pairs in a microstructure fiber,” *Opt. Lett.* **30**, 3368–3370 (2005).
  - [45] B. Huttner, S. Serulnik, and Y. Ben-Aryeh, “Quantum analysis of light propagation in a parametric amplifier,” *Phys. Rev. A* **42**, 5594–5600 (1990).
  - [46] J. Peřina Jr. and J. Peřina, “Quantum statistics of nonlinear optical couplers,” in *Progress in Optics, Vol. 41*, edited by E. Wolf (Elsevier, Amsterdam, 2000) pp. 361–419.
  - [47] J. Peřina Jr., “Waves in spatio-spectral and -temporal coherence of evolving ultra-intense twin beams,” *Sci. Rep.* **9**, 4256 (2019).
  - [48] A. Pieczonková and J. Peřina, “Statistical properties of Brillouin scattering,” *Czech. J. Phys. B* **31**, 837–856 (1981).
  - [49] A. V. Chizhov, “Stokes-anti-Stokes entanglement in stimulated Raman scattering,” *Physics of Particles and Nuclei Letters* **6**, 494 (2009).
  - [50] P. Sekatski, N. Sangouard, F. Bussières, C. Clausen, N. Gisin, and H. Zbinden, “Detector imperfections in photon-pair source characterization,” *J. Phys. B* **45**, 124016 (2012).
  - [51] S. Friberg, C. K. Hong, and L. Mandel, “Measurement of time delays in the parametric production of photon



- pairs,” *Phys. Rev. Lett.* **54**, 2011–2013 (1985).
- [52] A. Lukš, V. Peřinová, and J. Peřina, “Principal squeezing of vacuum fluctuations,” *Opt. Commun.* **67**, 149–151 (1988).
- [53] S. Hill and W. K. Wootters, “Computable entanglement,” *Phys. Rev. Lett.* **78**, 5022 (1997).
- [54] G. Adesso and F. Illuminati, “Entanglement in continuous-variable systems: recent advances and current perspectives,” *J. Phys. A* **40**, 7821 (2007).
- [55] M. Horodecki, P. Horodecki, and R. Horodecki, “Separability of mixed states: Necessary and sufficient conditions,” *Phys. Lett. A* **223**, 1–8 (1996).
- [56] A. Peres, “Separability criterion for density matrices,” *Phys. Rev. Lett.* **77**, 1413–1415 (1996).
- [57] C. T. Lee, “Measure of the nonclassicality of nonclassical states,” *Phys. Rev. A* **44**, R2775 (1991).
- [58] J. Peřina Jr., V. Michálek, and O. Haderka, “Higher-order sub-Poissonian-like nonclassical fields: Theoretical and experimental comparison,” *Phys. Rev. A* **96**, 033852 (2017).
- [59] E. G. Cavalcanti, S. J. Jones, H. M. Wiseman, and M. D. Reid, “Experimental criteria for steering and the Einstein-Podolsky-Rosen paradox,” *Phys. Rev. A* **80**, 032112 (2009).
- [60] I. Kogias, A. R. Lee, S. Ragy, and G. Adesso, “Quantification of Gaussian quantum steering,” *Phys. Rev. Lett.* **114**, 060403 (2015).
- [61] K. Banaszek and K. Wódkiewicz, “Nonlocality of the Einstein-Podolsky-Rosen state in the Wigner representation,” *Phys. Rev. A* **58**, 4345 (1998).
- [62] S. Olivares and M. G. A. Paris, “Enhancement of nonlocality in phase space,” *Phys. Rev. A* **70**, 032112 (2004).
- [63] J. F. Clauser, M. A. Horne, A. Shimony, and R. A. Holt, “Proposed experiment to test local hidden-variable theories,” *Phys. Rev. Lett.* **23**, 880 (1969).
- [64] C. A. Parra-Murillo, M. F. Santos, C. H. Monken, and A. Jorio, “Stokes–anti-Stokes correlation in the inelastic scattering of light by matter and generalization of the Bose-Einstein population function,” *Phys. Rev. B* **93**, 125141 (2016).
- [65] A. Jorio, M. Kasprczyk, N. Clark, E. Neu, P. Maletinsky, A. Vijayaraghavan, and L. Novotny, “Optical-phonon resonances with saddle-point excitons in twisted-bilayer graphene,” *Nano Lett.* **14**, 5687–5692 (2014).
- [66] M. Kasprczyk, A. Jorio, E. Neu, P. Maletinsky, and L. Novotny, “Stokes–anti-Stokes correlations in diamond,” *Opt. Lett.* **40**, 2393–2396 (2015).
- [67] J. Peřina and J. Křepelka, “Stimulated Raman scattering of squeezed light with pump depletion,” *J. Mod. Opt.* **38**, 2137–2151 (1991).
- [68] J. Peřina and J. Křepelka, “Joint probability distributions and entanglement in optical parametric processes,” *Opt. Commun.* **284**, 4941–4950 (2011).
- [69] P. M. Mose and H. Feshbach, *Methods of Theoretical Physics, Vol. 1* (McGraw–Hill, Amsterdam, 1953).
- [70] J. Peřina Jr., “Coherence and mode decomposition of intense twin beams,” *Phys. Rev. A* **92**, 013833 (2015).